High-Performance Polymer Semiconductors for Organic Thin-Film Transistors

by

Bin Sun

A thesis

presented to the University of Waterloo

in fulfillment of the

thesis requirement for the degree of

Master of Applied Science

in

Chemical Engineering

Waterloo, Ontario, Canada, 2012

Author's Declaration

I hereby declare that I am the sole author of this thesis. This is a true copy of the thesis,

including any required final revisions, as accepted by my examiners.

I understand that my thesis may be made electronically available to the public.

Abstract

A novel polymer semiconductor with side chains thermally cleavable at a low temperature of 200 °C was synthesized. The complete cleavage and removal of the insulating 2-octyldodecanoyl side chains were verified with TGA, FT-IR, and NMR data. The N-H groups on the native polymer backbone are expected to form intermolecular hydrogen bonds with the C=O groups on the neighboring polymer chains to establish 3-D charge transport networks. The resulting side chain-free conjugated polymer is proven to be an active p-type semiconductor material for organic thin film transistors (OTFTs), exhibiting hole mobility of up to 0.078 $cm^2V^{-1}s^{-1}$. This thermo-cleavable polymer was blended with PDQT to form films that showed a higher performance than the pure individual polymers in OTFTs.

MoO_3 or NPB was used as a hole injection buffer layer between the metal electrodes and the polymer semiconductor film layer in OTFT devices. This buffer layer improved hole injection, while its use in the OTFT, improved the field-effect mobility significantly due to better matched energy levels between the electrodes and the polymer semiconductor.

Acknowledgements

This research project would not have been possible without the support of the following people: first and foremost I wish to appreciate my supervisors, Prof. Yuning Li and Prof. Hany Aziz, who were abundantly helpful and offered invaluable assistance, support and guidance. Deepest gratitude is also due to my thesis reviewers, Prof. Mark Pritzker and Prof. Zhongwei Chen, without their knowledge and assistance this study would not have been successful.

Deep thanks also to all my lab mates: Dr. Wei Hong, Dr. Jonathan Yuen, Chang Guo, Leanne Murphy, and Jane Yan, for their help with my experiments. Special gratitude to Dr. Denise Gosselink, Dr. Feng Chen, and Jian Zhang, who helped me tremendously with my experiments.

I also wish to express my gratitude to my family and friends who have been constantly providing support and help.

Contents

List of Figures

List of Schemes

List of Tables

List of Abbreviations

OFET: Organic field effect transistor

OTFT: Organic thin film transistor

AFM: Atomic force microscopy

FT-IR: Fourier transform infrared spectroscopy

UV-Vis: Ultraviolet–visible spectroscopy

XRD: X-ray diffraction

NMR: Nuclear magnetic resonance spectroscopy

TMS: tetramethylsilane

PDQT: poly(2,5-bis(2-octyl-1-dodecyl)-3,6-di(thiophen-2-yl)pyrrolo[3,4-*c*]pyrrole-1,4(2*H*,5*H*)-dione-alt-2,2'-bithiophene)

PDQT-tc: poly(2,5-bis(2-octyldodecanoyl)-3,6-di(thiophen-2-yl)pyrrolo[3,4-*c*]pyrrole-1,4(2*H*,5*H*)-dione-alt-2,2'-bithiophene)

PDQT-n: poly(3,6-di(thiophen-2-yl)pyrrolo[3,4-*c*]pyrrole-1,4(2*H*,5*H*)-dione-alt-2,2'-bithiophene)

PDBFBT: 3,6-Di(furan-2-yl)pyrrolo[3,4-*c*]pyrrole-1,4(2*H*,5*H*)-dione and bithiophene copolymer

THF: Tetrahydrofuran

NMP: *N*-Methyl-2-pyrrolidone

DMSO:　Dimethyl sulfoxide

PR:　photo resist

Chapter 1 Introduction

1.1 Overview

A transistor is a semiconductor device used to control the flow of electrical current (electronic signal) between two terminals of transistor by applying and switching an input voltage or current on a third terminal. Since the output power can be higher than the input power, the transistor can work as a signal amplifier to provide a current or voltage gain. Transistors are commonly used as electronic switches to show "on" or "off" signals both for high-power applications such as switched-mode power supplies and for low-power applications such as logic gates.

In 1947, John Bardeen and Walter Brattain at Bell Labs observed that when two gold point contacts were applied to a crystal of germanium, a signal was produced with the output power greater than the input. William Shockley worked to greatly expand the knowledge of transistors.[1] For their contribution to the field of semiconductor and their discovery of semiconductor transistors, William Shockley, John Bardeen, and Walter Brattain were awarded the 1956 Nobel Prize in Physics.

In 1954, Gordon Teal in Texas Instruments produced the first silicon transistor.[2] The first metal–oxide–semiconductor (MOS) transistor was built by Kahng and Atalla at Bell Labs in 1960. In a very short period of time, transistors replaced vacuum tubes for use in integrated circuits for the controlling appliances and machinery. Transistors play an important role in all modern electronics, especially in computers.

In 1930, the field-effect transistor (FET) was first proposed by J.E. Lilienfeld,[3] and the first field-effect transistor was designed and prepared by Kahng and Atalla using a metal-

oxide-semiconductor in 1960.[4] A field-effect transistor is a transistor that uses an electric field to control the conductivity of a channel of one type of charge carrier in a semiconductor material to provide a current as on/off signal or to amplify the current. Figure 1.1 shows a field effect transistor with a top contact and bottom gate structure, where the gate controls the current between the source and drain electrodes, similar to the switching of a tap to control the water flow. The source (S) is the electrode where the majority carriers enter the channel and the drain (D) is the electrode where the majority carriers leave the channel. The gate (G) is the terminal electrode that controls the channel conductivity. By controlling the gate voltage, the drain current can be tuned.
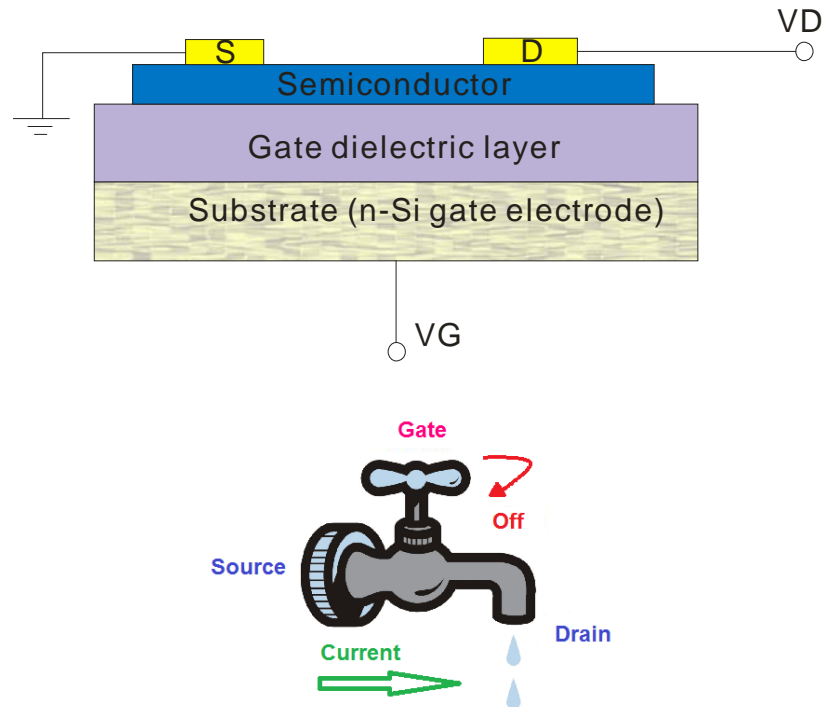
Figure 1.1 Field effect transistor with a structure of top contact and bottom gate (top); analogous control of water flow by tap operation like transistor.

However, high costs of the silicon semiconductor and device fabrication have led researchers to find more desirable materials such as organic semiconductors. In 1987, Koezuka and his co-workers reported the first organic field-effect transistor (OFET),[5] which was based on polythiophene, a typical organic polymer semiconductor. OFETs can be prepared from small molecules by vacuum evaporation or from polymers by solution processing (casting or spin-coating). The excellent solution processibility of organic semiconductors open up potential applications in radio-frequency identification (RFID) tags, flexible displays, electric paper, organic memory and photovoltaics due to the low cost in large area processing without the need of a high vacuum environment and high temperatures during fabrication.[6-9] Figure 1.2 shows some applications of organic field effect transistors.
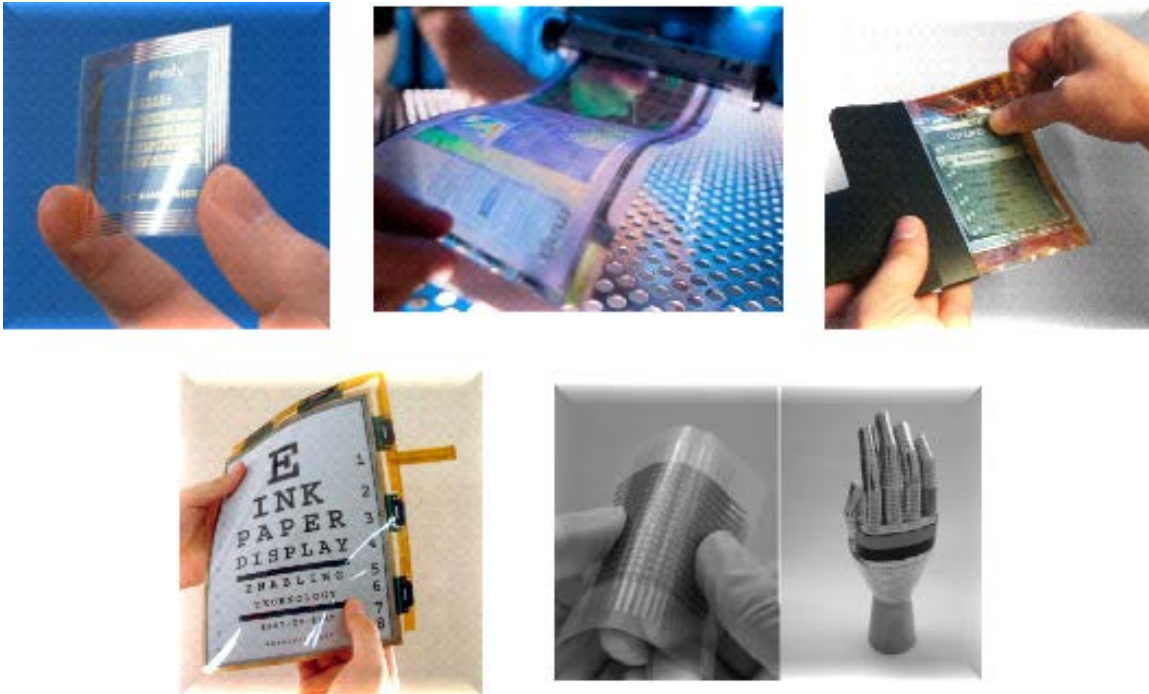
Figure 1.2 Application of organic field effect transistor in plastic RFID, flexible displays, paper phone, electronic paper and sensors. [10-14]

1.2 Organic Thin-film Transistor (OTFT)

OFETs are now designed and fabricated as thin film devices that are also called thin-film transistors (OTFTs). The structure of OTFTs is similar to that of the metal oxide semiconductor field-effect transistors (MOSFETs) based on silicon.
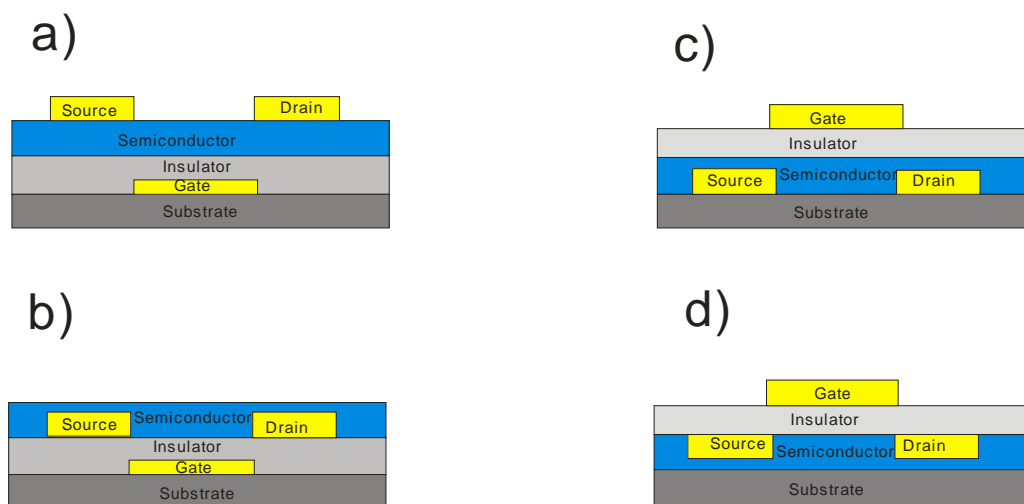
Figure 1.3 OTFT device structure: a) top-contact device with source and drain electrodes deposit on the organic semiconducting layer; b) bottom-contact bottom gate device with the organic semiconductor deposited onto the gate insulator and the pre-evaporated source and drain electrodes on gate dielectric layer; c) bottom-contact device with the organic semiconductor deposited onto the pre-evaporated source and drain electrodes and followed by gate dielectric layer and gate electrode deposition; d) top-contact top gate device with source and drain electrodes evaporated on the organic semiconducting layer and then covered by insulator and gate electrode.

Figure 1.3 shows four common device configurations used in OTFTs. Figure 1.4 shows a typical 3-D configuration of OTFTs, where W is the channel width and L is the channel length. When a sufficient voltage is applied to the gate, a conductive channel is formed,

through which a current between source and drain flows (holes for p-type semiconductor and electrons for n-type semiconductor) with a drain voltage (V_D). The *I-V* characteristics of OTFTs can be described by models developed for inorganic semiconductors. PDQT [29] OTFTs in Figure 1.5 are used here to demonstrate typical *I-V* characteristics of OTFTs and the methods used to calculate the field effect mobility.
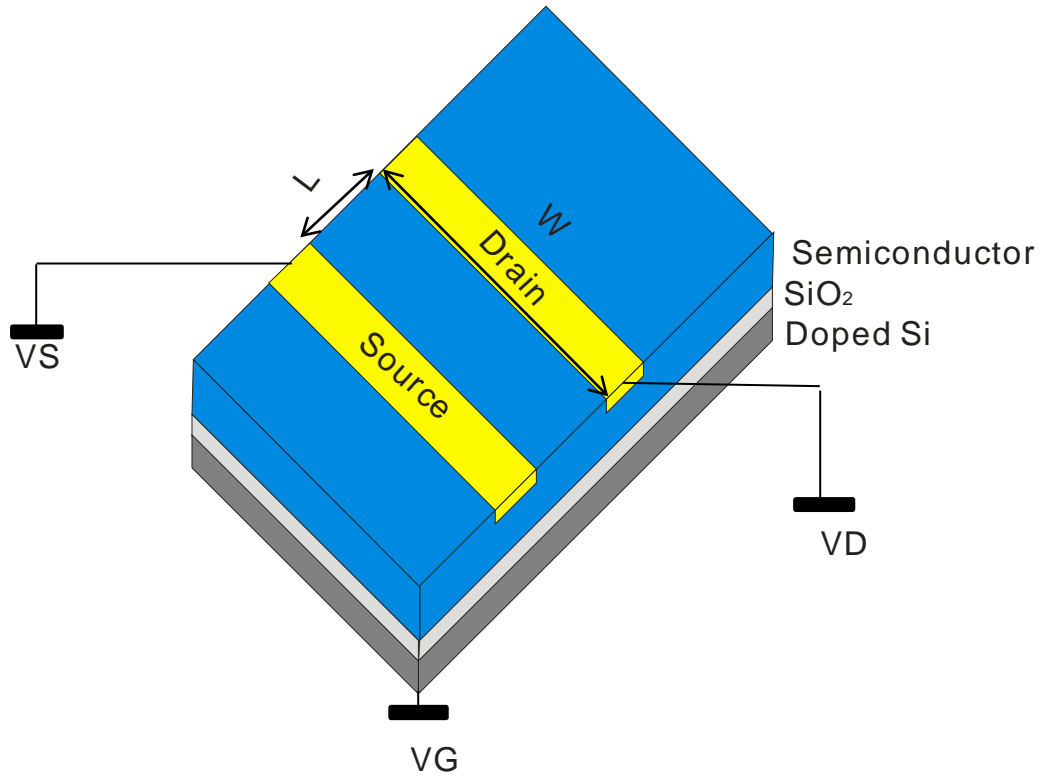
Figure 1.4 3-D structure of bottom gate/ top contact device of OTFT
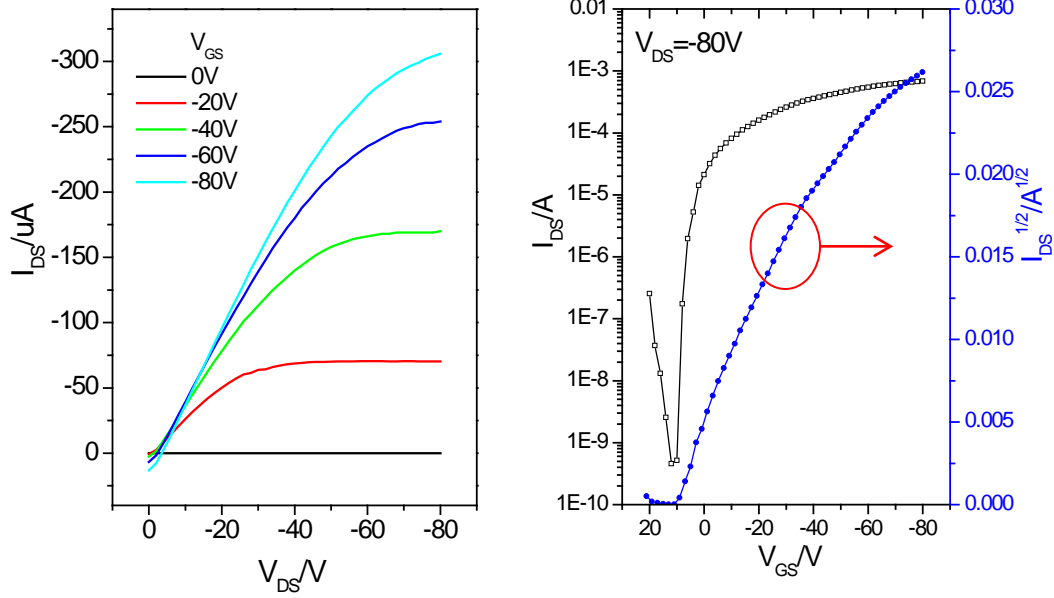
Figure 1.5. Output of hole accumulation regimes (left); Transfer characteristics (right). OTFT is fabricated by employing the bottom contact (Au electrode) structure on doped p-silicon wafers. 200nm SiO$_2$ layer (capacitance 17nF/cm^2) on the p-silicon wafer was used as the gate insulator. The polymer film was obtained by spin-coating on substrate with a thickness of 40nm. Channel length L=30um and channel width W=1mm. The saturation mobility is 1.3 cm^{2}V^{-1} s^{-1} at VD=-80V.

Figure1.5-left shows output characteristics for different gate voltage values. The ohmic (linear) behavior at low drain voltages and drain current saturation above the pinch-off point appears shown in output curves. The data can be fitted in both the linear (1) and saturation regions (2) as follows:

$$I_{DS} = \mu C_i \frac{W}{L}((V_{GS} - V_T) - \frac{V_{DS}}{2})V_{DS} \ (1)$$

$$I_{DS} = \mu C_i \frac{W}{2L}(V_{GS} - V_T)^2 \ (2)$$

where I_{DS} is the drain-source current, W is the channel width, C_i is the gate insulator capacitance density (F/cm^2), V_{GS} is the gate-source voltage, and V_T is the threshold voltage. These equations are valid for a long channel length. A long channel length

means the gate electric field is much larger than the longitudinal electric field, which is normally greater than 10 μm. Otherwise the drain current to the saturation voltage ($\frac{dI_{DS}}{dV_{DS}}$) above pinch-off will not be zero. [16] In the saturation regime, mobility can be calculated from the slope of the plot of $\sqrt{I_{DS}}$ versus V_{GS}. In Figure 1.5-right, the graph contains semilogarithmic plot I_{DS} versus V_{GS} and a plot of $\sqrt{I_{DS}}$ versus V_{GS}. It corresponds to a bottom contact / bottom gate OTFT with a channel length L=30um and a channel width W=1mm comprising PDQT as the semiconductor layer with a 200nm SiO_2 as the gate dielectric layer and heavily doped p-silicon as the gate electrode and gold source and drain electrodes. The saturation mobility is 1.3 cm^2V^{-1} s^{-1}, which is calculated from the slope of the $\sqrt{I_{DS}}$ versus V_{GS} plot (V_{GS} from 8V to -2V). It is important to note that the W/L value of this OTFT device is about 33, which is much higher than 10. With such as high W/L ratio, the effects of fringe currents flowing outside the channel could be minimized to avoid an overestimate of the mobility. While the threshold voltage V_T is +8.6V, and the I_{on}/I_{off} ratio is about 1.5×10^6 when V_{GS} was scanned from +20V to -80V.

1.3 Conjugated polymer semiconductors

Polymer semiconductors have attracted much attention in recent years as active materials in organic thin film transistors (OTFTs) due to the low cost solution process (solution casting, ink-printing or spin-coating) as used for their fabrication. [34-38]

The first polymer-based OTFTs reported in 1987 [5] showed mobility of ~10^{-5} $cm^2V^{-1}s^{-1}$. In the last few years, several new polymer semiconductors with mobilities above 1 $cm^2V^{-1}s^{-1}$ in OTFTs have been reported, which are better than amorphous silicon semiconductor.

In some recent work, it was found that semiconducting polymers which combine electron donating (D) and accepting (A) building blocks in the main backbone are one of the most promising and attractive classes of conjugated polymers for high performance (mobility) in OTFT application.[17-19] A D–A system induces intermolecular D–A interactions, leading to increased molecular ordering through self-assembly of the polymer main chains and forming polymer networks through donor-acceptor (D-A) interactions for highly efficient charge transport. Figure 1.6 and 1.7 show some important acceptor and donor chemical structures. Selection of D–A building blocks for a conjugated polymer backbone requires considering the electron donating and accepting capability, planarity, chemical-electrochemical stability, and efficient tunability in electronic characteristics through side chain substitution, solubility and solid state self-assembly. D–A combination allows scientist to tune the band gap through hybridization of the highest occupied molecular orbital (HOMO) of the donor moiety with the lowest unoccupied molecular orbital (LUMO) of the acceptor to fit the requirement of organic electric application. For example, the HOMO level could be tuned to be below -5 eV for p-type carrier transport and LUMO level to be below -4 eV for n-type transport.
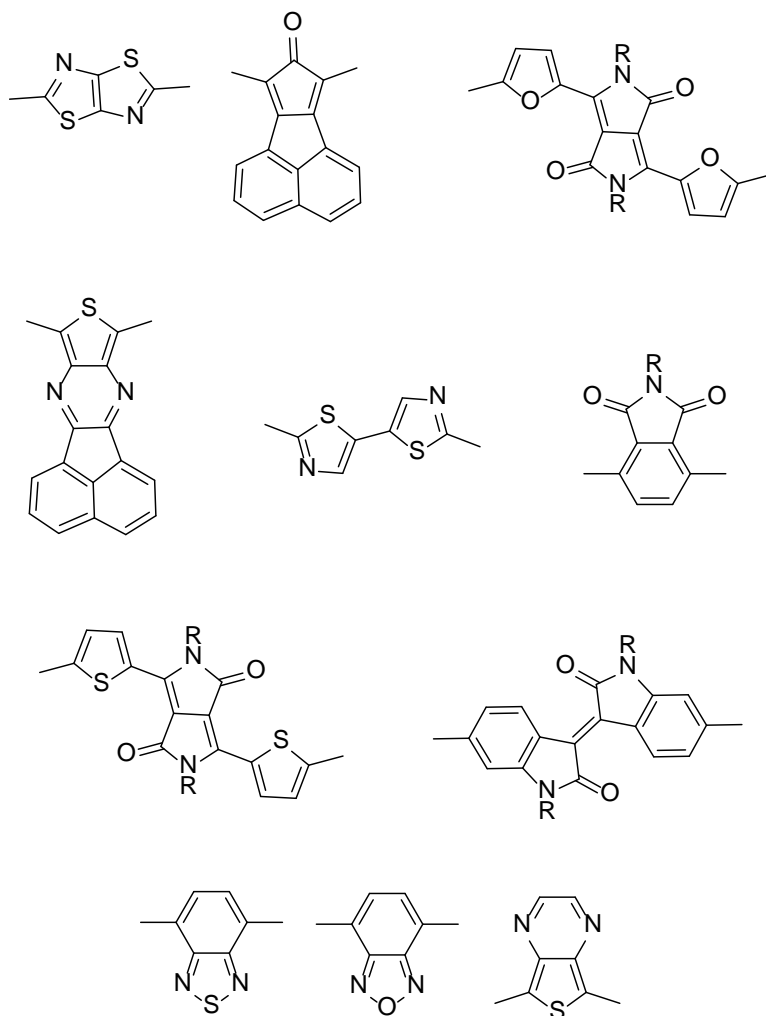
Figure 1.6 Important building blocks to construct polymer acceptors
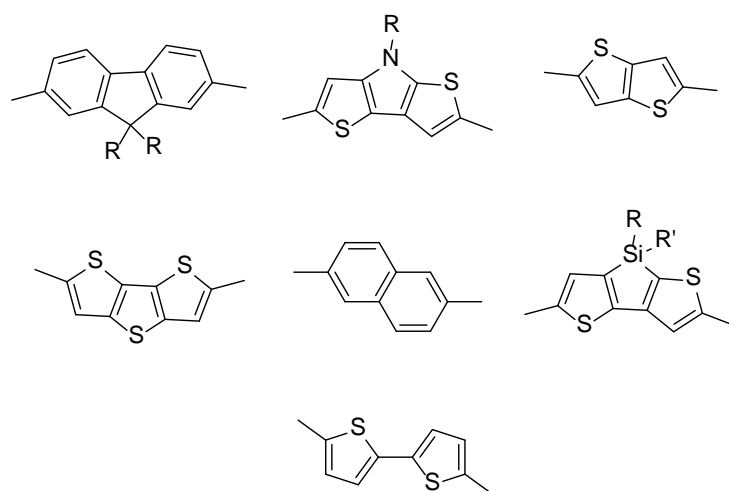
Figure 1.7 Important chemical heterocycles to construct polymer donors

Combinations of these donors and acceptors gave polymers with high hole mobilities of 0.11-1.2 $cm^2V^{-1} s^{-1}$. [20-24]

Pei and coworkers [25] first reported the use of an isoindigo-based polymer combining with a bi-thiophene unit to yield a hole mobility of 0.79 $cm^2V^{-1} s^{-1}$. The structure of this polymer is shown in Figure 1.8 -left.
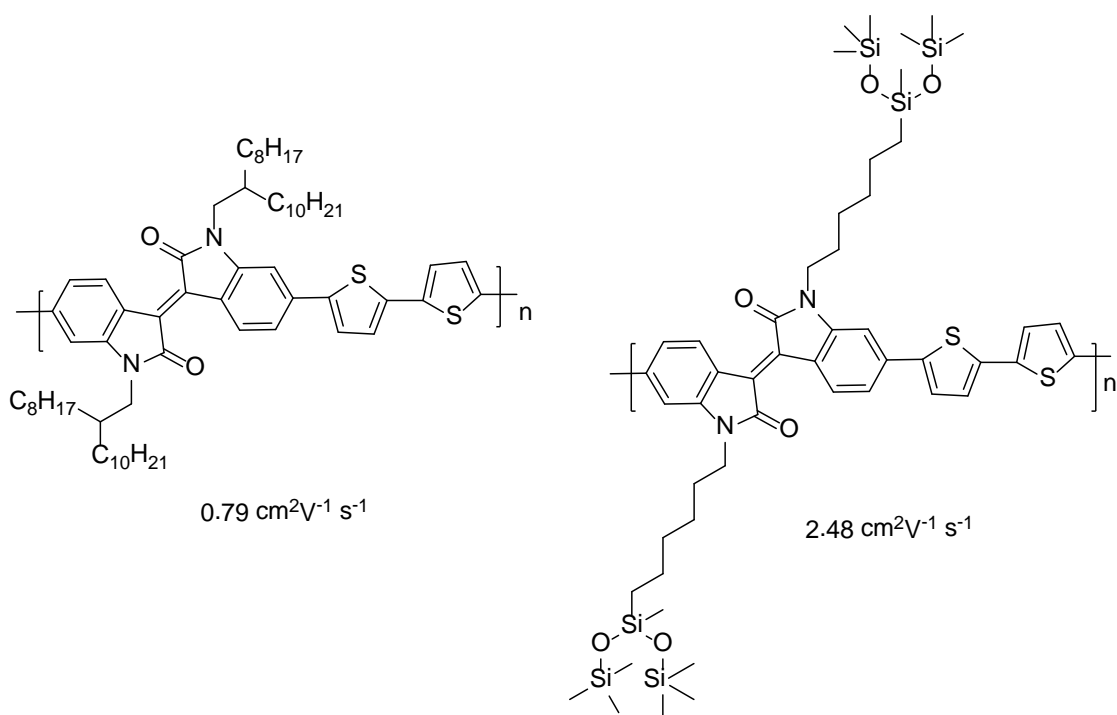
Figure 1.8 Isoindigo based polymer with high hole transport mobility

Later, Bao's group [26] reported an impressive result with a hole transport mobility of up to 2.48 $cm^2V^{-1} s^{-1}$ with a new silicon-containing side-chain (Figure 1.8-right).

Our group has focused on diketopyrrolopyrrole (DPP)-based polymer. This building block has been used extensively to combine with other donor building blocks to form

various D–A copolymers. Several DPP-containing polymers have achieved carrier mobilities close or over 1 cm^{2}V^{-1} s^{-1}. [15]

PDQT [29]
0.97 cm^{2}V^{-1} s^{-1}

PDPP-TNT [30]
0.98 cm^{2}V^{-1} s^{-1}

PDBT-co-TT [27,28]
0.94-1.62 cm^{2}V^{-1} s^{-1}

PDPP-TBT [31]
0.35(hole)/0.40(electron) cm^{2}V^{-1} s^{-1}

PDVT-10 [32]
8.2 cm^{2}V^{-1} s^{-1}

Figure 1.9 Representative DPP-based polymer semiconductors for OTFTs.

In 2010, our group reported a new DPP-based polymer with a donor of thieno[3,2-*b*]thiophene, showing high hole mobility of 0.94 cm^2V^{-1} s^{-1} in OTFTs with a bottom gate and top contact structure. This high mobility could arise from the strong intermolecular interactions due to π-π stacking, donor-acceptor interaction and the ordered lamellar structure. [27] When the polymer film was tested in top gate structure, the hole mobility could reach as high as 1.62 cm^2V^{-1} s^{-1}, which shows a potential to improve the performance of conjugated polymers in OTFT applications.[28] The highly efficient charge transport is attributed to the strong intermolecular D-A interactions and the larger π-π overlap of the planar thieno[3,2-*b*]thiophene units. The former effect brings the polymer chains closer, reaching a very short π-π distance of 3.71 Å, while the latter provides ample charge hopping channels along the π-π stacks.

A DPP-based copolymer having a bithiophene donor with a hole mobility in OTFT of 0.97 cm^2V^{-1} s^{-1} was reported in 2011 by our group[29]. This polymer forms ordered lamellar packing even without thermal annealing, when annealed at a mild temperature of 100 °C the thin film showed similarly high mobility of 0.89 $cm^2V^{-1}s^{-1}$. This may be because of the strong intermolecular interactions from the fused aromatic DPP moiety and the DPP−QT donor−acceptor interaction forming a large π−π overlap, which are favorable for intermolecular charge hopping.

Later, our group reported a novel donor–acceptor co-polymer, PDPP-TNT, based DPP acceptor and fused naphthalene donor. This structure naphthalene is attached through 1,4-, 1,5- or 2,6-positions to the conjugated backbone. This polymer showed a hole mobility of 0.98 cm^2V^{-1} s^{-1} in bottom gate and dual gate OTFTs.[30] Additionally, PDPP–TNT, which has a HOMO (5.29 eV) energy level and optimum optical band gap (1.50 eV), is a

promising candidate for organic photovoltaic (OPV) applications, and gave high power conversion efficiencies (PCE) of 4.7% in OPV devices with an acceptor $PC_{71}BM$.

In 2010, our group also reported a new ambipolar DPP-based copolymer with a benzothiadiazole donor building block in its backbone. This resulted in ambipolar charge transport in OTFT devices with balanced hole and electron mobilities of 0.35 cm^2V^{-1} s^{-1} and 0.40 cm^2V^{-1} s^{-1}, respectively.[31] Very recently, Liu and coworkers reported a new DPP-based polymer with a DPP acceptor unit and a (*E*)-2-(2-(thiophen-2-yl)vinyl)thiophene (TVT) donor unit, which exhibited a very high hole mobility of 8.2 cm^2V^{-1} s^{-1}.[32]

Therefore, diketopyrrolopyrole (DPP) is a promising building block for high performance D-A polymer semiconductor organic thin film transistors with high mobility, and organic photovoltaic (OPV) with a high power conversion efficiencies.

1.4 Conclusion

In this chapter, the background and operation of organic thin film transistors were introduced, and common device configurations and evaluation of devices briefly discussed. Polymer semiconductors are the most ideal choice due to their excellent solution processability in a variety of solvents. Equally important are their mechanical robustness, light weight and flexibility. Due to the high mobility of the D-A polymers, they have become very competitive with small molecular organic semiconductors and amorphous silicon semiconductors.

Chapter 2   DPP-based semiconducting polymer bearing thermocleavable side chains

2.1 Introduction

π-conjugated polymer semiconductors have attracted much attention in recent years as active materials in organic thin film transistors (OTFTs),[34-38] organic photovoltaics (OPVs),[39-44] etc. Their excellent solution processability and mechanical robustness allow for fabrication of various low-cost, large-area, and flexible organic electronic products such as displays, radio-frequency identification (RFID) tags, memory devices, and solar cells.[6-9] To be solution-processable, a large portion of solubilizing side chains must be incorporated to oppose the strong aggregation tendency of polymer backbones from solution. For instance, the hexyl side chains in poly(3-hexylthiophiophene) (P3HT) constitute up to ~51% of the polymer mass. The non-conjugated side chains would separate the semiconductive aromatic polymer backbones and intrinsically reduce the overall charge carrier transport performance. Labile side chain groups, which provide the needed solubility and can be chemically [45-48] or thermally [49-58] removed under mild conditions, have been used to substitute both small molecular and polymeric semiconductors to achieve a higher density of the aromatic components via a post-deposition thermal treatment. For example, cyclohexadiene4a and N-sulfinylamide4b were used to form soluble pentacene precursors, which can undergo thermally activated retro-Diels-Alder reactions to recover the native semiconductive pentacene after solution deposition. Fréchet *et al*. used thermally decomposable secondary ester groups as

terminal substituents for oligothiophenes.[51, 52] After thermal annealing, the resulting oligothiophenes possessed shorter terminal groups and showed good performance in OTFTs. The same research group reported a polythiophene having tertiary ester side chains, which form carboxylic acid side chains upon heating at 210 °C.[54] To form a completely side chain-free (native) polythiophene, a higher temperature of 310 °C is required to remove the carboxylic acid groups.[56] Bao and co-workers recently found that the secondary or tertiary alkyl groups on the nitrogen atoms of quaterrylene diimides could be removed at elevated temperatures (~350-400 °C) with the chromophore intact.[53] After thermally removing the side chains, the resulting quaterrylene diimide showed a significant increase in mobility in OTFTs. Holdcroft et al reported polythiophenes having side chains comprising acid-sensitive tetrahydropyran (THP) groups.[45-48] In the presence of a trace amount of acid and at an elevated temperature, the THP groups are readily detached to enable closer polymer packing due to the shortened side chains.[45] The THP group was also found thermocleavable at ~300 °C.[54, 58]

Here we report a novel polymer semiconductor, PDQT-tc, which has 2-octyldodecanoyl side chains that can be completely thermally decomposed at a low temperature of ~200 °C to form a side-chain-free conjugated polymer PDQT-n. Our results show that this native conjugated polymer is a promising semiconductor for OTFTs and other organic electronics.

2.2 Results and Discussion

The key building block for PDQT-tc is 2,5-dihydro-pyrrolo[3,4-c]pyrrole-1,4-dione or diketopyrrolopyrrole (DPP), which has been an increasingly popular electron acceptor moiety for high mobility donor-acceptor polymers in OTFTs.[15, 27, 29-31, 60-62] *tert*-Butoxycarbonyl (*t*-BOC) substituted DPP molecule was found to be thermally decomposable at ~180 °C.[63] Very recently a DPP-based copolymer incorporating a BOC-DPP unit was reported.[64] The BOC groups in the polymer could be thermally removed at ~200 °C and the resulting polymer showed enhanced electron transport performance. Previously we have developed a high mobility polymer PDQT,[29] which has solubilising 2-octyldodecyl (OD) side chains on the DPP units. In this study, we synthesized a PDQT derivative, PDQT-tc, which has 2-octyldodecanoyl groups on the nitrogen atoms. The synthesis of PDQT-tc is outlined in Scheme 2.1 2,5-Dihydro-3,6-di-2-thienyl-pyrrolo[3,4-c]pyrrole-1,4-dione (1) was first substituted with 2-octyldodecanoyl groups at two nitrogen atoms by reacting with NaH in *N*-methylpyrrolidone (NMP), followed by addition of 2-octyldodecanoyl chloride, yielding 2,5-bis(2-octyldodecanoyl)-2,5-dihydro-3,6-di-2-thiophen-pyrrolo[3,4-c]pyrrole-1,4-dione (2) in ~10% yield. Bromination of 2 with 2 equivalents of *N*-bromosuccinimide (NBS) gave 3,6-bis(5-bromothiophen-2-yl)-2,5-bis(2-octyldodecanoyl)-2,5-dihydro-pyrrolo[3,4-*c*]pyrrole-1,4-dione (3) in 65% yield. Stille coupling polymerization of 3 with 5,5'-bis(trimethylstannyl)-bithiophene was conducted in toluene at 90 °C for 24 hr in the presence of a catalytic amount of bis(triphenylphosphine)palladium(II) dichloride. The resulting crude polymer was purified by Soxhlet extraction sequentially with acetone and hexane to remove oligomers and other impurities. Extraction with chloroform dissolved

the remaining polymer, affording blue solid films after removal of solvent with a high yield of 92%. The number average molecular weight (M_n) and polydispersity index (PDI) of PDQT-tc were determined by gel-permeation chromatography (GPC) to be 24,334 and 3.90, respectively, using chlorobenzene as an eluent and polystyrene as standards at a column temperature of 40 °C.
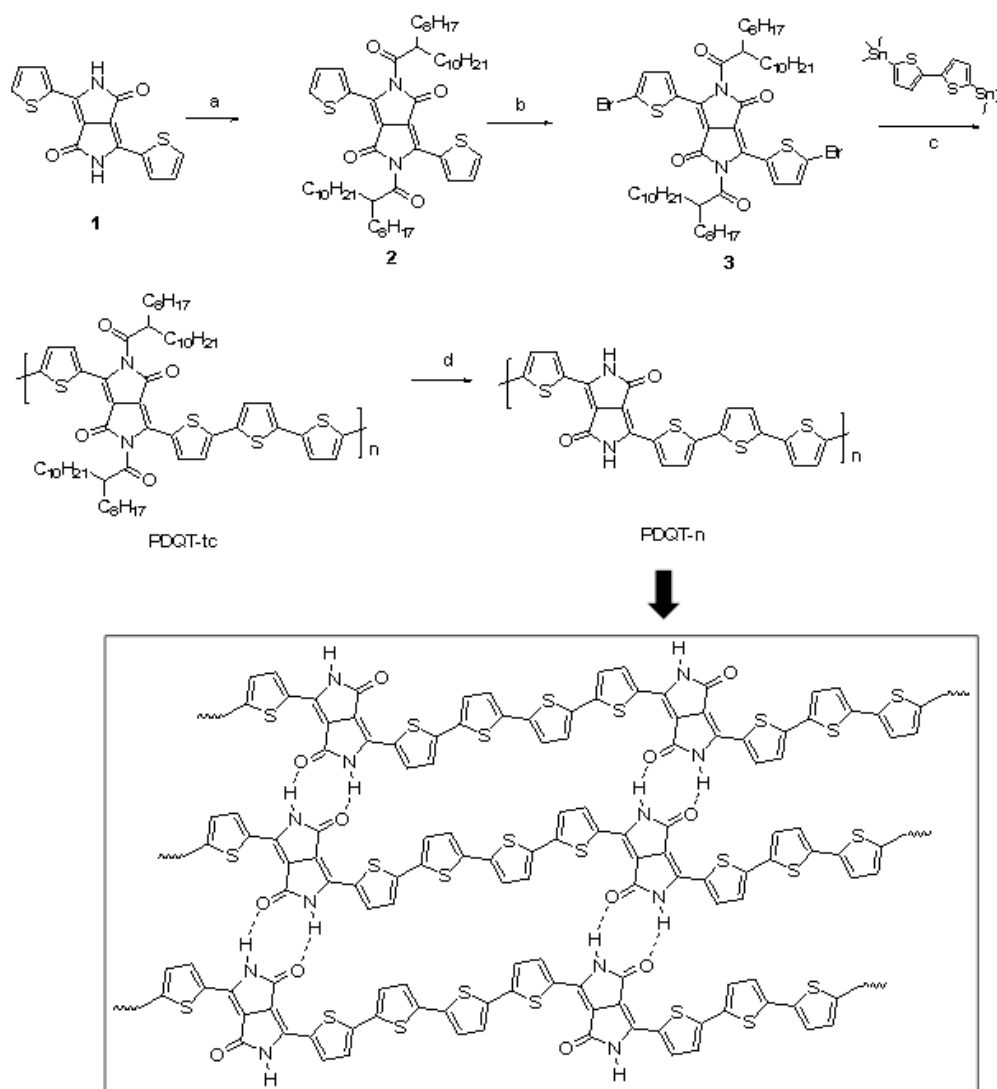
Scheme 2.1 Synthesis of PDQT-tc and PDQT-n: a) i)NaH, NMP, ii) 2-octyldodecanoyl chloride; b) NBS, CHCl$_3$; c) Pd(PPh$_3$)$_2$Cl$_2$, toluene, 90 °C ; d) heating at T = 200 °C under nitrogen.

The thermal decomposition characteristics of PDQT-tc were investigated by using the thermogravimetric analysis (TGA). The thermal liability of the –N-C(=O)- was demonstrated by heating compounds 2 and 3. Both compounds started to decompose at ~180 °C, although compound 3 was found to decompose at a slightly faster rate (Figure 2.1). Polymer PDQT-tc started to lose weight at ~200 °C, while its structural analogue PDQT,[29] which has 2-octyldodecyl side chains, showed a much higher onset thermal decomposition temperature at ~400 °C. The weight loss of at ~46% PDQT-tc levelled off at ~46% by ~350 °C, which is ~10% less than the calculated mass fraction (~56%) of the 2-octyldodecanoyl side chains in PDQT-tc. This discrepancy is probably due to trapping of some decomposed side chain fragments in the polymer sample, on the other hand, the decomposed side chains could evaporate readily.
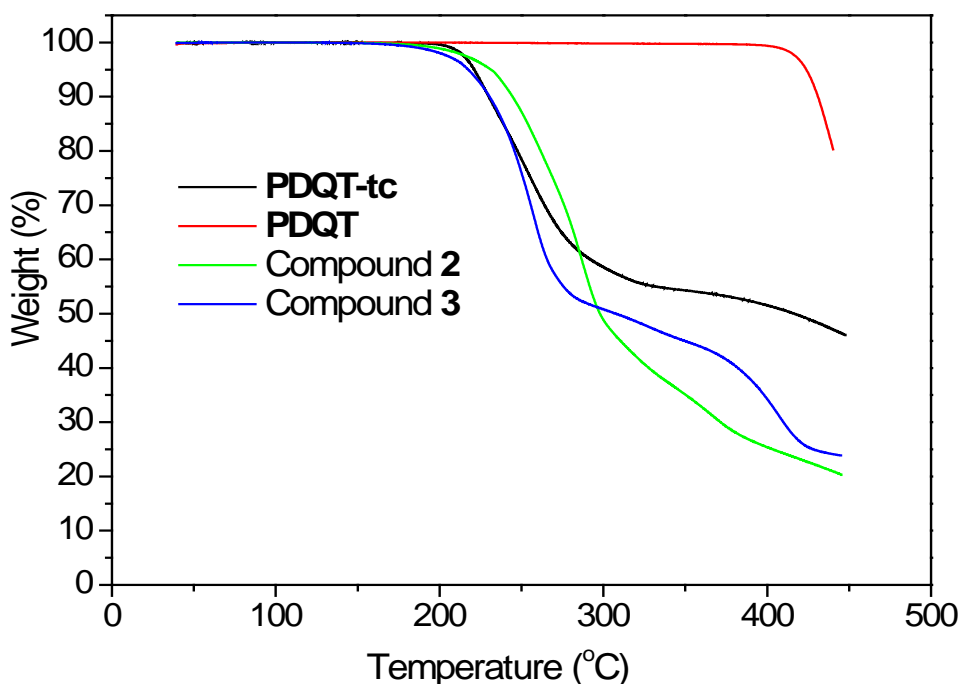
Figure 2.1 TGA curves of PDQT-tc, PDQT, compound 2, and compound 3 at a heating rate of 10 °C min^{-1} under nitrogen.
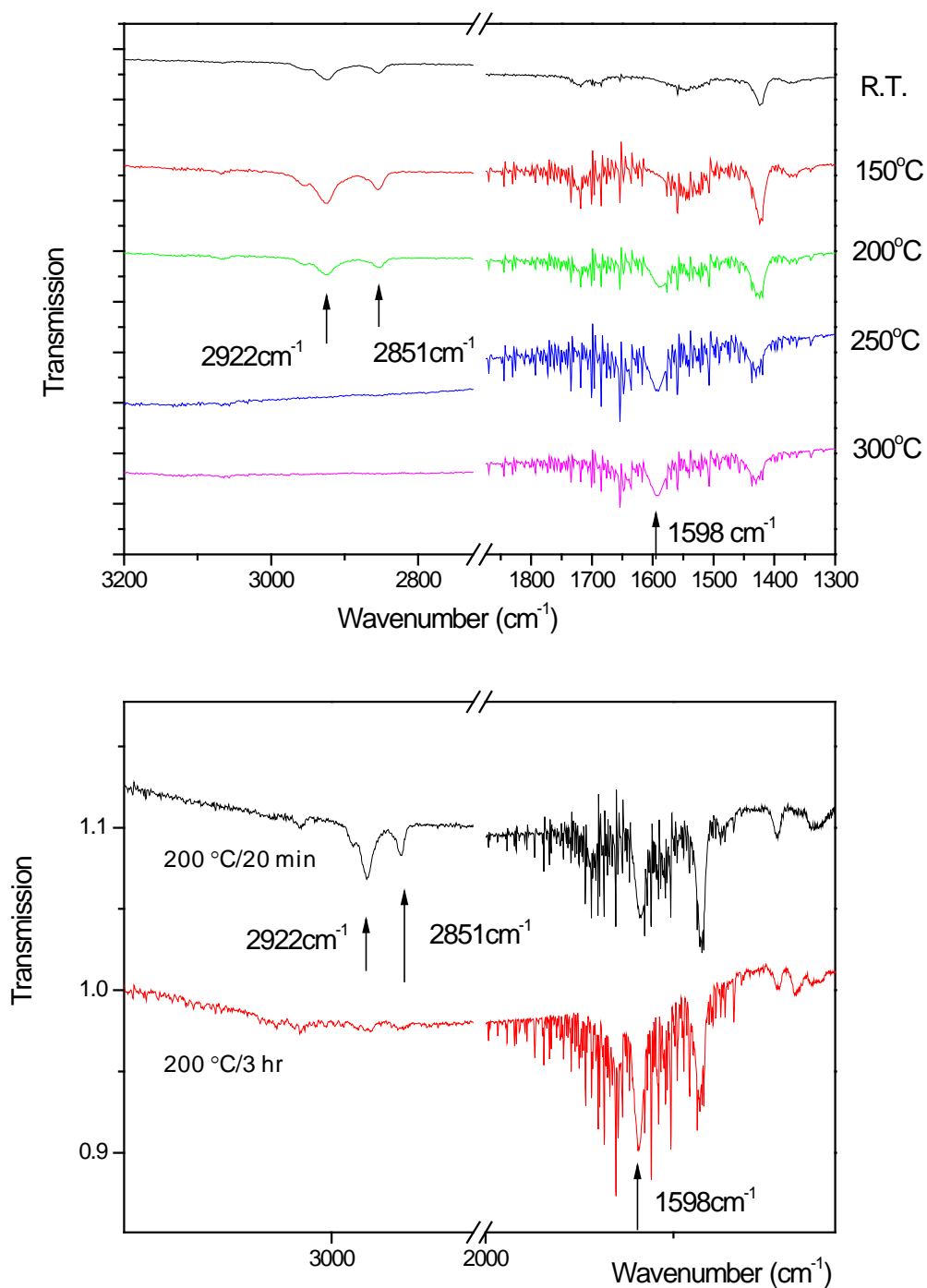
Figure 2.2 Top: FT-IR spectra of PDQT-tc films on Si wafer annealed at different temperatures for 20 min in nitrogen. Bottom: FT-IR spectra of PDQT-tc films on Si wafer at 200 °C for 20 min and 3 hr, respectively.

The chemical structural changes of PDQT-tc upon heating were studied by FT-IR. The thin film samples (~63 nm in figure 2.7) for FT-IR measurements were prepared by spin coating a PDQT-tc solution in chloroform on boron-doped silicon wafer substrates with a (111) orientation and a resistivity of ~10 Ωcm, followed by thermal annealing in a glove box filled with nitrogen for 20 min at various temperatures. It can be clearly seen that the peaks (2922 and 2851 cm^{-1}) representing the side chain C-H groups decreased upon heating at ~200 °C and completely disappeared after heating at 250 °C or higher (Figure 2.2: top). It was also observed that a peak at 1598 cm^{-1}, which originated from the N-H vibration, appeared with film annealed at 200 °C. By extending the annealing time to 3 hr, the side chains could be completely removed at 200 °C (Figure 2.2: bottom). The thickness of the polymer films with side chains completely removed is ~26 nm, which is ~41% of the thickness (~63 nm) of the films prior to thermal treatment (Figure 2.3). This reduction has an agreement with the calculated value (44%), assuming that the density of the polymer before and after thermal annealing remains similar. As opposed to the trapping of some decomposed side chains observed in the TGA experiments, the complete elimination of side chains of PDQT-tc confirmed by FT-IR is likely due to the easier evaporation of the decomposed side chain fragments in the thin films used for the FT-IR measurements than in the bulk samples used for the TGA. The liberated N-H groups in the resulting PDQT-n without side chains are expected to strongly interact with the C=O groups on the DPP units of the neighbouring polymer chains by intermolecular hydrogen bonding (NH•••O),[65, 66] which would form tightly held three-dimensional networks of native semiconducting polymer backbones (Scheme 2.1). Figure 2.4 showed PDQT-tc film was very stable, even annealed at at 150 °C for 20hr.
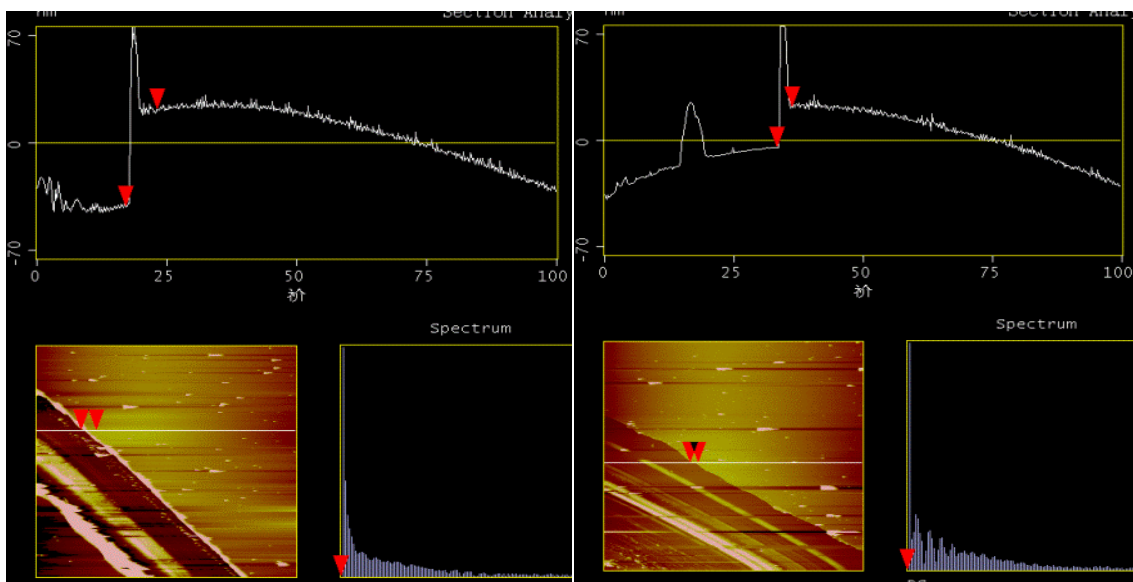
Figure 2.3 Film thickness analysis of **PDQT-tc** thin films using AFM: left) before (63 nm) and right) after (26 nm) thermal annealing at 200 °C for 3 hr.
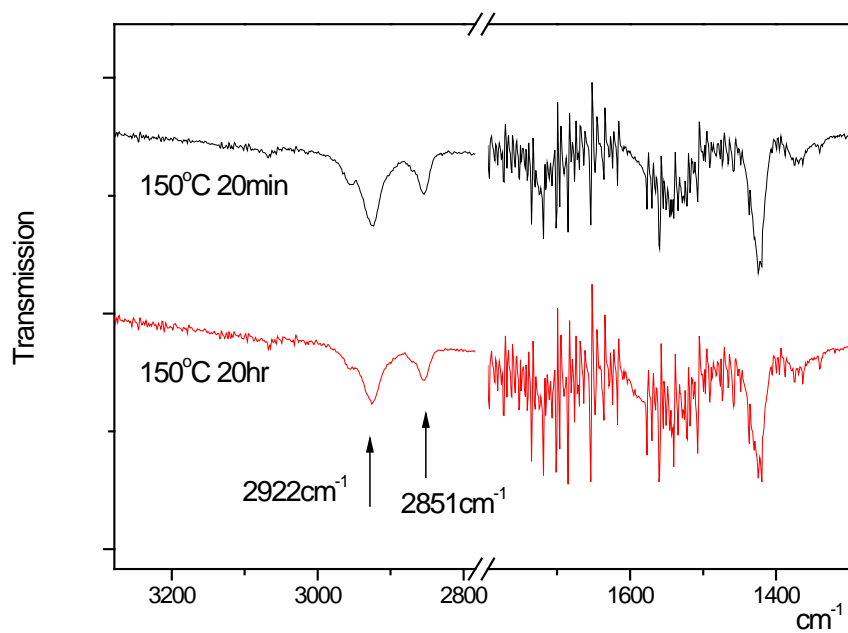
Figure 2.4 FT-IR spectra of PDQT-tc films on Si wafer annealed at 150 °C for 20 min and for 20hr in nitrogen.
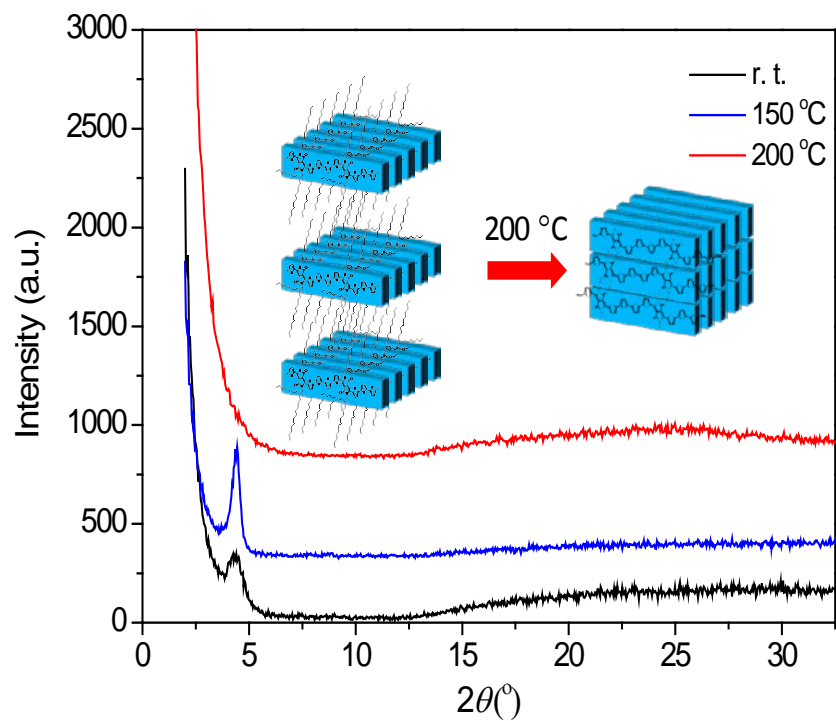
Figure 2.5 XRD diagrams obtained from PDQT-tc thin films on DTS- treated SiO_2 /Si substrates annealed at 150 °C for 20 min and 200 °C for 3 h in nitrogen along with the one of the as-spun thin film (r. t.).
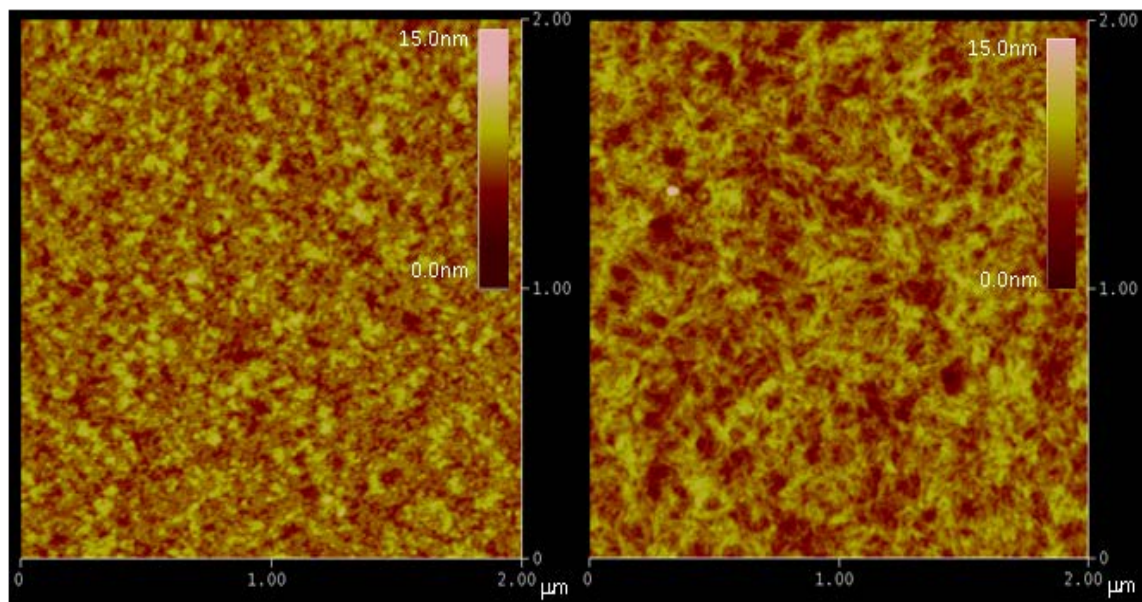
Figure 2.6 AFM images (2 µm × 2µm) of PDQT-tc thin films annealed at 150 (left) for 20 min and 200 °C (right) for 3hr in nitrogen. The root mean square (RMS) roughness of the films is 0.89nm (left) and 1.42 nm (right).

The X-ray diffractometry (XRD) measurements of the as-spun film and the films annealed at 150 and 200 °C are shown in Figure 2.5. The as-spun film showed a diffraction peak at 2θ= ~4.40°, which corresponds to a d-spacing of 20.1 Å. This spacing corresponds to the inter-lamellar distance observed for PDQT.[29] The much weaker diffraction intensity for PDQT-tc is probably due to the presence of the C=O groups on the 2-octyldodecanoyl side chains, which interfere with the molecular ordering. The primary peak of the thin film annealed at 150 °C became intensified, due to the improved molecular ordering. After annealing at 200 °C for 3 hr, this diffraction peak completely disappeared. This is due to the elimination of the side chains, which results in the shortening of the interlayer distance. It is also noted that the diffraction intensity in the broad range from ~15 to 30° increased, which is possibly associated with the formation of an amorphous phase. Atomic force microscopic (AFM) images in Figure 2.6 show that the PDQT-tc film annealed at 150 °C (without removal of side chains) is quite smooth (with an RMS roughness of 0.89 nm), and comprised of small nanograins (~20-30 nm). After removal of side chains by annealing at 200 °C for 3 hr, the nanograins in the resulting PDQT-n film are connected to form nanofibers. The film becomes rougher (with an RMS roughness of 1.42 nm) and has large gaps (~10's-100's nm) between domains.
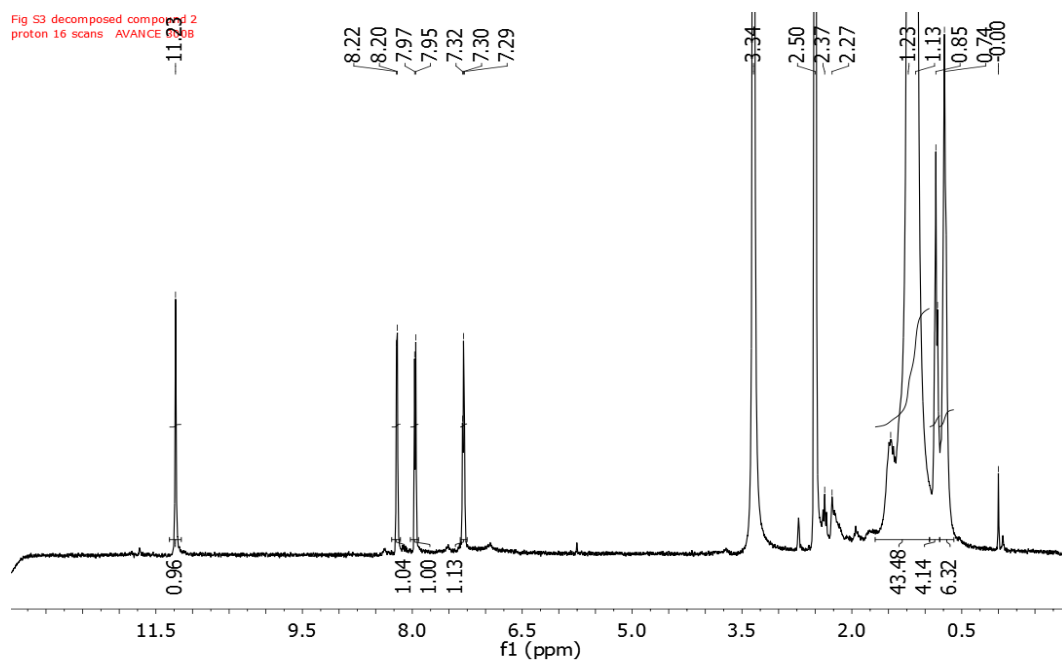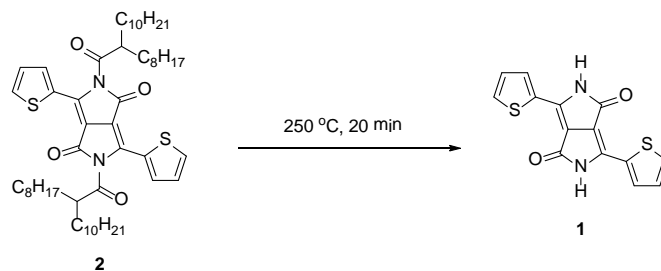
Figure 2.7 300 MHz ¹HNMR of the mixture of the decomposed compound **2** at 250 °C for 20 min measured in DMSO-*d6*. It can be clearly seen that the aromatic peaks of compound **2** disappeared completely and the aromatic peaks corresponding to those of compound **1** appeared.
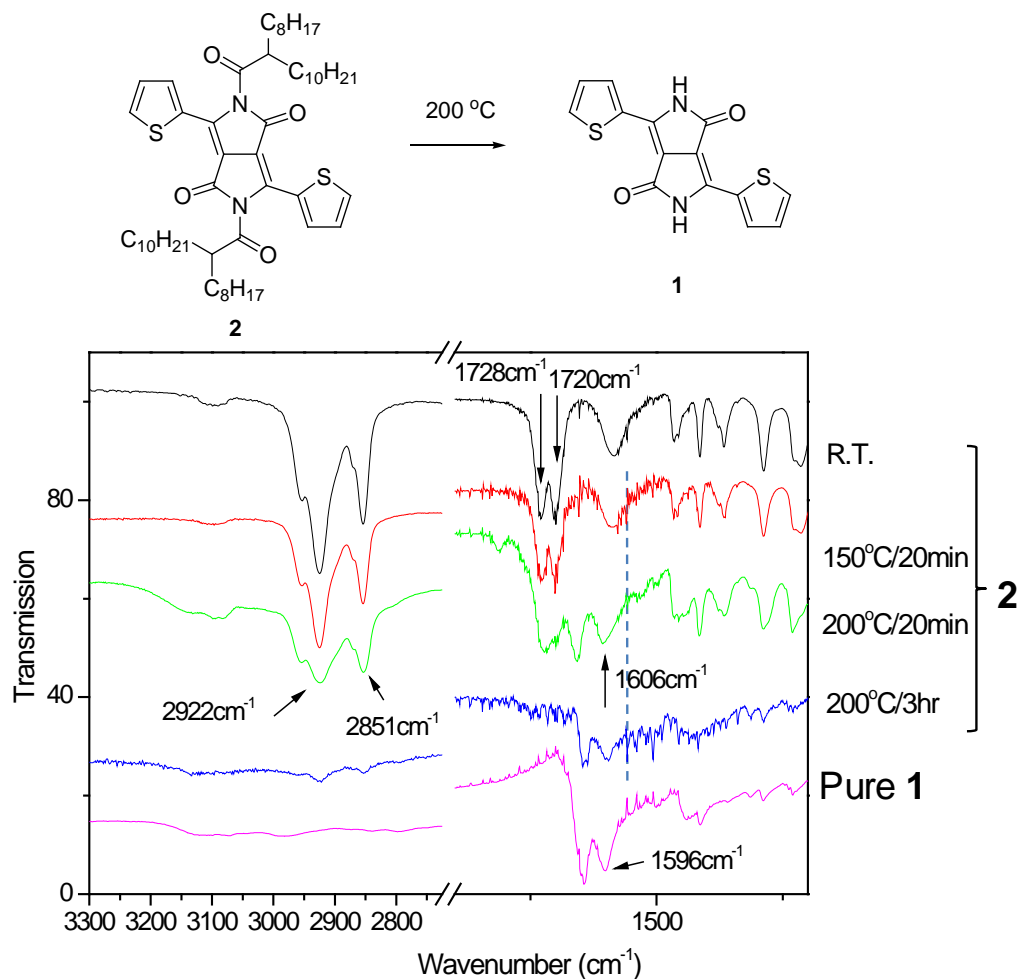
Figure 2.8 Top: The proposed thermal decomposition reaction of compound **2** to form compound **1**. Bottom: FT-IR spectra of pure compound **1** on a KBr substrate and compound **2** films on Si wafer substrates annealed at different temperatures in nitrogen.

The side chain-free PDQT-n films are insoluble in any solvents for NMR analysis. To indirectly elucidate the chemical structure of PDQT-n, compound 2 was thermally decomposed at 250°C for 20 min in a sealed vial on a hotplate. The mixture after heating was analyzed using ^{1}H NMR in Figure 2.7, which unambiguously showed that compound 2 is completely decomposed and the new peaks appeared in the aromatic region are identical to the peaks of the known compound 1 in Figure 2.11 with free N-H groups. The

thermal decomposition of compound 2 to form compound 1 was also investigated using

In Figure 2.8 bottom, FT-IR spectra of pure compound 1 on a KBr substrate and

compound 2 films on Si wafer substrates annealed at different temperatures in nitrogen.

The intense peaks at 2922 cm^{-1} and 2851 cm^{-1} of the non-annealed 2 originate from the

stretching vibrations of the side chain C-H bonds, which decreased significantly after

heating at 200 °C for 3 hr. The peaks at 1728 and 1720 cm-1 are from the stretching

vibrations of the C=O groups on the 2-octyldodecanoyl substituents of compound 2,

which disappeared after heating at 200 °C for 3 hr. The new peak appeared at 1596 cm^{-1}

in the thin film annealed at 200 °C for 3hr is due to the bending of the N-H groups of the

recovered compound 1.   The spectrum of the sample annealed at 200 °C for 3 hr

resembles the one of the pure compound 1, indicating that compound 2 was thermally

decomposed to form compound 1, as shown in Figure 2.4 top. Therefore it is reasonable

to assume that PDQT-tc was converted into the side chain-free native conjugated polymer

PDQT-n as proposed in Scheme 2.1.
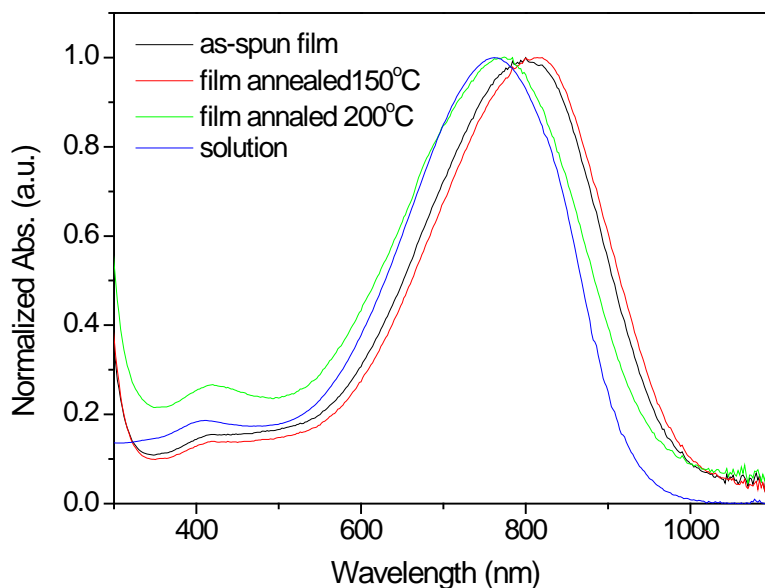
Figure 2.9 UV-Vis spectra of the PDQT-tc chloroform solution and thin films on glass substrates without annealing (as-spun), annealed at 150 °C for 20 min, and annealed at 200 °C for 3 hr in nitrogen.

The UV-Vis absorption spectra of PDQT-tc in a chloroform solution and thin films are shown in Figure 2.9. In solution, PDQT-tc exhibited an absorption maximum (λ_{max}) at 762 nm. The as-spun thin film showed a λ_{max} at a longer wavelength of 800 nm, suggesting improved coplanarity of the polymer backbone and chain packing order. Thermal annealing at 150 °C led to a further red-shift in the λ_{max} to 820 nm. When the annealing temperature was increased to 200 °C, the absorption peak of the resulting PDQT-n film was significantly blue-shifted to 772 nm. This dramatic change suggests the shortening of the effective π-conjugation length of the polymer chains, which is probably the direct result of the formation of a less ordered, amorphous phase where the polymer backbones are rather twisted. The strong interchain hydrogen bonding between the C=O and the N-H groups of the native conjugated backbones in the PDQT-n film might have segregated the π-π stacks during the elimination of the side chains. The resulting backbone-only polymer PDQT-n would have very strong intermolecular interactions, which inhibit any chain motion to reorganize the polymer chains into ordered crystalline structures.

PDQT-tc was tested in bottom-gate, top-contact OTFT devices. A heavily p-doped silicon wafer with a ~200-nm thermally grown SiO_2 layer was used as the substrate, where the conductive silicon functions as the gate electrode and the SiO_2 layer as the dielectric. The SiO_2 layer was modified with dodecyltrichlorosilane (DTS) prior to use. A PDQT-tc solution in chloroform was spin coated on the substrate at 1500 rpm for 60 s to

form a ~60-70-nm polymer thin film, which was subjected to thermal annealing at 200 °C for 3 hr in a glove box to form a ~30nm PDQT-n thin film. Then the source-drain electrode pairs were deposited on top of the polymer thin film by thermal evaporation of silver through a shadow mask to form OTFT devices with a channel width (W) of 4 mm and a channel length (L) of 100 µm. For comparison, OTFT devices using PDQT-tc annealed at 150 °C for 20 min (without eliminating the side chains) were fabricated. All devices were encapsulated with a TiO_x top layer,[62] which was deposited by spin coating a precursor solution and then annealing at 80 °C for 20 min. The devices were characterized in air and in the dark.
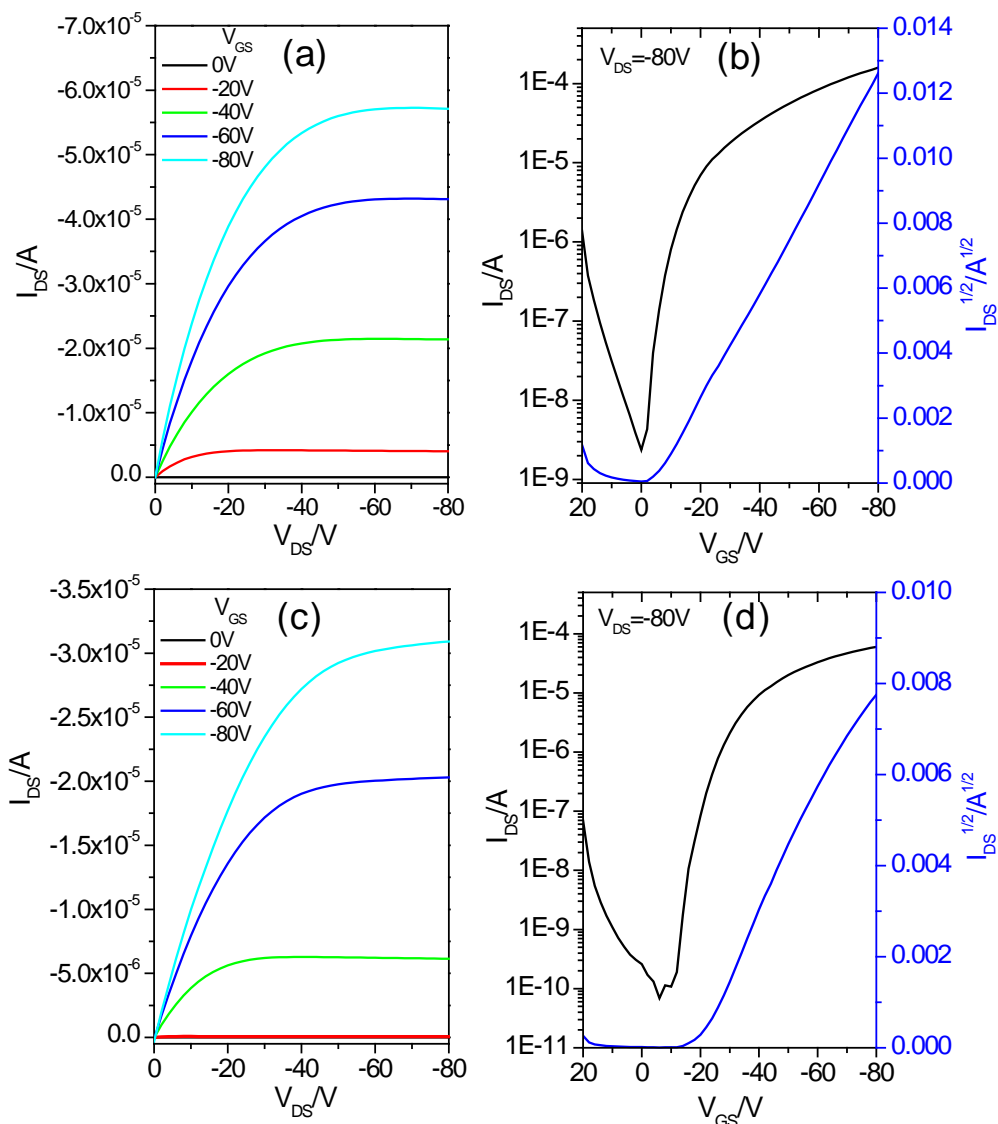
Figure 2.10 Output and transfer curves of an OTFT device with a PDQT-tc thin film annealed at 150 °C for 20 min (a and b) and an OTFT device with PDQT-n obtained by heating a PDQT-tc thin film at 200 °C for 3 hr in nitrogen (c and d). Device dimensions: channel width (W) =4 mm; channel length (L) =100 μm.

As shown in Figure 2.10, the device with PDQT-tc annealed at 150 °C showed typical hole transport characteristics under the hole accumulation (enhancement) mode. The hole mobility in the saturation regime is 0.096 $cm^2V^{-1}s^{-1}$ in the saturation regime with a current on-to-off ratio of 8.6 ×10^5. The mobility value is about one order of magnitude

lower than that of PDQT, probably due to the poor crystallinity of the polymer thin film. The device having the PDQT-n film obtained by annealing a PDQT-tc film at 200 °C for 3 hr also showed a typical hole transport behaviour. The hole mobility of this device is 0.078 cm^{2}V^{-1}s^{-1}, slightly lower than that of the device annealed at 150 °C. However, if the amorphous nature of the PDQT-n film is taken into account, the charge transport of this polymer is quite efficient. It will be our next subject of study to maintain the crystallinity and the π-π stacking during the thermal elimination of the side chains by fine-tuning the heating profile. Thermal removal of side chains under a high pressure [53] will also be used to improve the quality and the crystallinity of the final native polymer thin film.

2.3 Experimental

2.3.1 Instrumentation and materials

All materials were purchased from Sigma-Aldrich and used without further purification. NMR data were collected on a Bruker DPX 300 MHz spectrometer with chemical shifts relative to tetramethylsilane (TMS, 0 ppm). FT-IR spectra were performed on FTIR-8400S (Shimadzu) Fourier Transform Infrared Spectrophotometer. UV-Vis spectra were recorded on a Thermo Scientific GENESYS™ 20 Spectrophotometer. XRD diagrams of polymer thin films (~100 nm) on the DTS-modified Si/SiO$_2$ substrate deposited by spin-coating polymer solutions in chloroform were obtained with a Bruker D8 Advance powder diffractometer using standard Bragg-Brentano geometry with Cu Kα radiation (λ = 1.5406 Å). Gel-permeation chromatography (GPC) measurements were performed on a Waters Breeze HPLC system using chlorobenzene as an eluent with polystyrene as standards at column temperature of 40 °C. Thermogravimetry analysis (TGA) was

conducted on a TGA Q500 (TA Instruments) at a heating rate of 10 °C min^{-1} under nitrogen. AFM images were performed on polymer thin films on DTS-modified SiO2/Si substrate using a Dimension 3100 Scanning Probe Microscope. The polymer thin films (~30-40 nm) were deposited by spin-coating polymer solutions in chloroform and optionally annealed at different temperatures.

2.3.2 Synthesis of 3,6-di(thiophen-2-yl)pyrrolo[3,4-*c*]pyrrole-1,4(2*H*,5*H*)-dione [67]
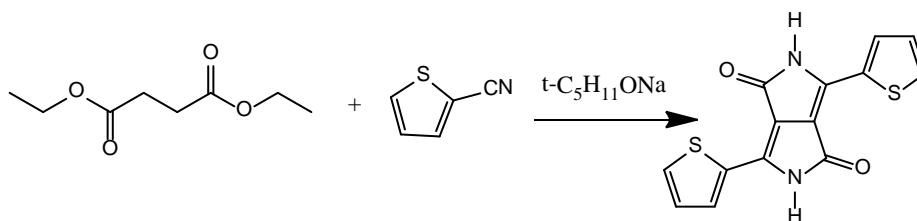
15.6g of sodium was added to 240mL 2-methyl-2-butanol and then the mixture was heated to 95°C. Then 49.3g thiophene-2-carbonitrile was added to the mixture when all the sodium was consumed. Finally, a solution containing 34.8g of diethyl succinate in 20mL of 2-methyl-2-butanol was added to the mixture drop-wise at 85 °C. The solution was stirred overnight and then cooled down to 50 °C. 150mL methanol was added to the solution. Then 60mL acetic acid was added drop-wise to neutralize the solution. Dark red precipitate appeared and the mixture became too viscose to stir. A glass rod was required to stir the precipitate before the magnet stirrer would work once again. After the mixture cooled down, the mixture was filtered. The red solid was washed by methanol, and then by water three times. This produced a brown solid that was then put in 600mL

isopropanol, and stirred for 3days. The final brown solid was obtained by filtering and drying. This procedure generated 40g product, corresponding to 66.7% yield.

^{1}H NMR (DMSO- d_6): 11.20, 8.18-8.17, 7.93-7.92, 7.28-7.25. (Figure 2.11)
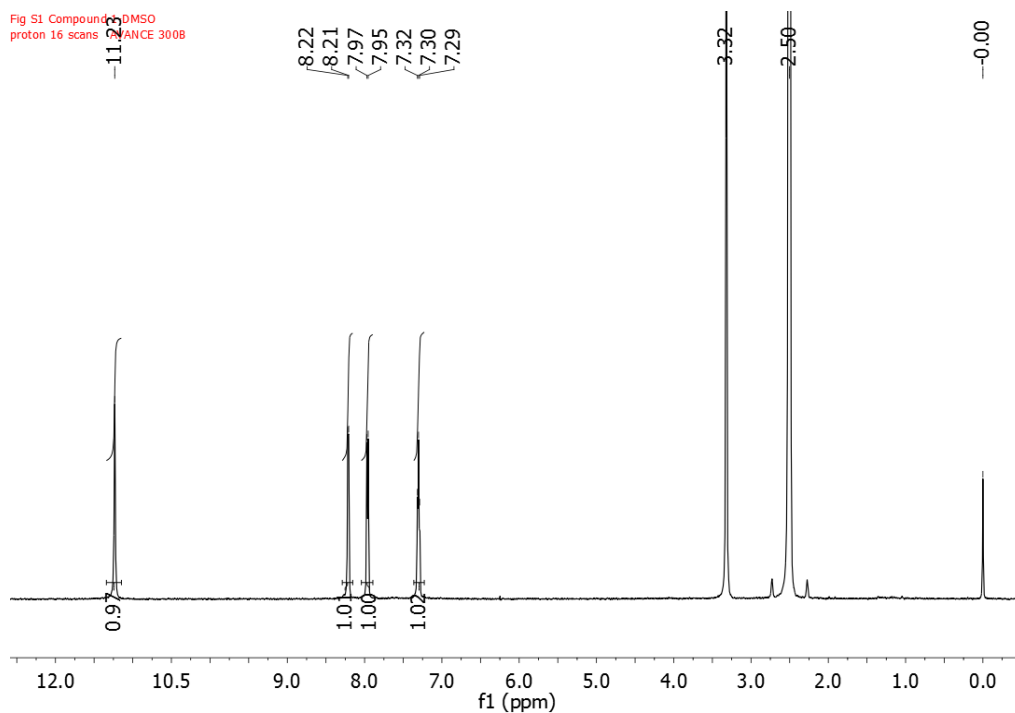
Figure 2.11 300 MHz ^{1}H NMR of the mixture of the compound 1, 3,6-di(thiophen-2-yl)pyrrolo[3,4-c]pyrrole-1,4(2H,5H)-dione

2.3.3 Synthesis of 2-octyldodecanoic acid
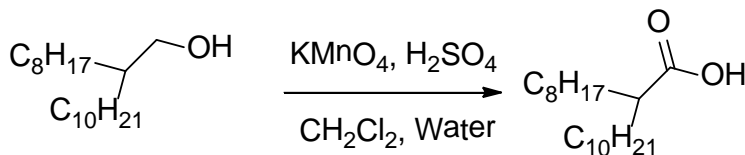
Sulphuric acid (10 g, 98%) was diluted with water (75 ml) and added to a solution of 2-octyl-1-dodecanol (30 g) in dichloromethane (60 ml). To this mixture 1M potassium permanganate solution (15 mL) was added drop-wise over 1 hr and then stirred for an additional 3 hr. The mixture was filtered to remove manganese dioxide precipitate,

washed with water, and treated with 2M NaOH (400 mL). The solution was washed with hexane, neutralized with 2M HCl, and extracted with ethyl acetate three times. The combined organic phase was dried over anhydrous Na_2SO_4. Distillation under a reduced pressure gave a colourless liquid (23g, 74%).

^{1}H NMR ($CDCl_3$) 2.38-2.35, 1.59-1.54, 1.47-1.43, 1.26, 0.90-0.85. (Figure 2.12)
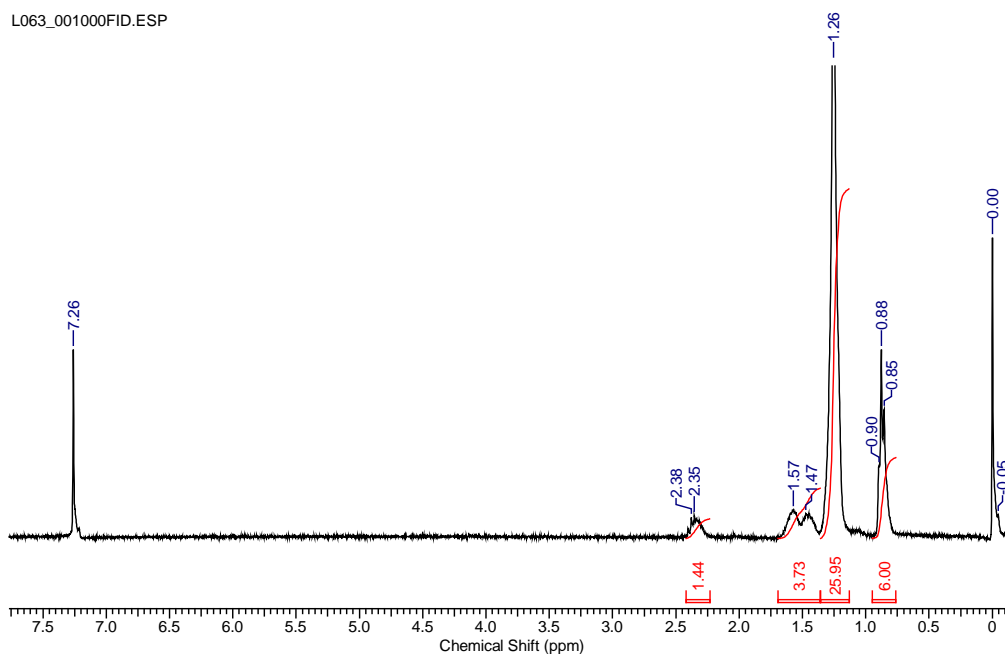
Figure 2.12 300 MHz ^{1}H NMR spectrum of 2-octyldodecanoic acid in $CDCl_3$

2.3.4 Synthesis of 2-octyldodecanoyl chloride
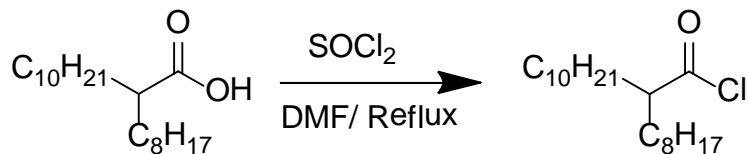
2-Hexyldecanoic acid (82 mmol, 21g) was added drop-wise into thionyl chloride (80 mL). The reaction mixture was refluxed for 3 hr and the excess thionyl chloride was

33

removed at 70 °C in vacuo to leave a brown liquid (22.3g, ~100%)), which was used in the next step without further purification.

^{1}H NMR (CDCl$_3$): 2.76-2.71, 1.70, 1.53, 1.24, 0.88-0.84. (Figure 2.13)
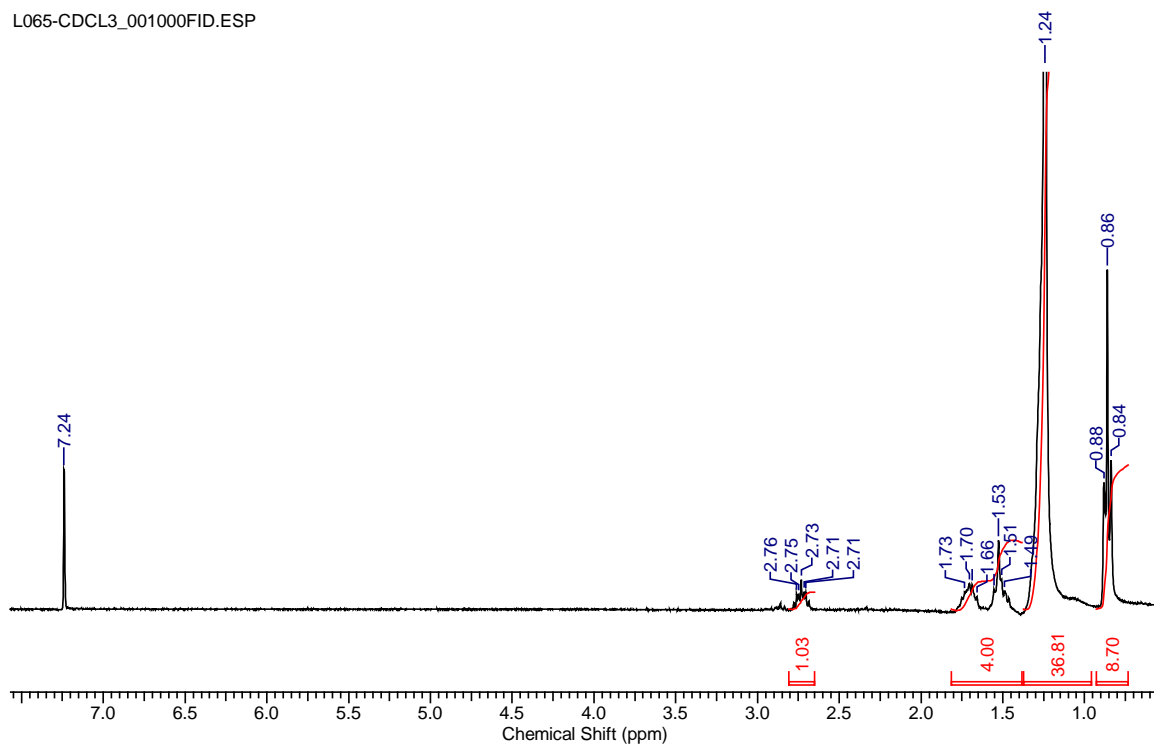
Figure 2.13 300 MHz ^{1}H NMR spectrum of 2-octyldodecanoyl chloride in CDCl$_3$

2.3.5 Synthesis of 2,5-bis(2-octyldodecanoyl)-3,6-di(thiophen-2-yl)pyrrolo[3,4-c]pyrrole-1,4(2H,5H)-dione (2)
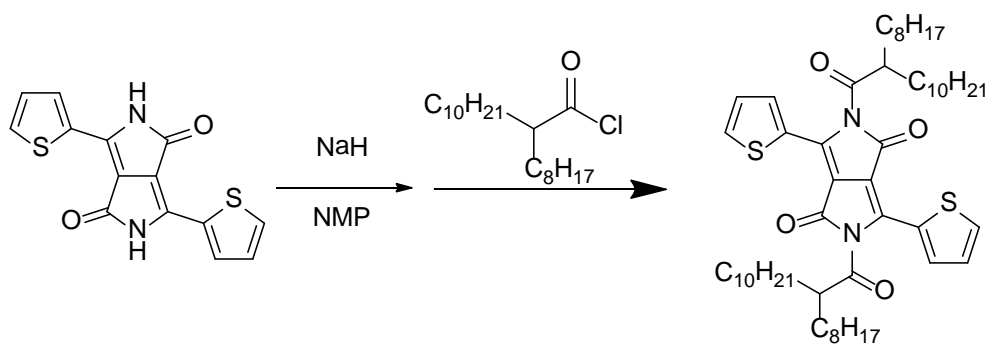
3,6-Di(thiophen-2-yl)pyrrolo[3,4-c]pyrrole-1,4(2H,5H)-dione (1) (1.2g, 4 mmol) was dissolved in anhydrous N-methyl-2-pyrrolidone (NMP) (25mL) at 60 °C. After the solution was cooled down to room temperature, and sodium hydride (0.36g, 9 mmol) was added. The reaction mixture was stirred for 0.5 hr at 60 °C before 2-octyldodecanoyl chloride (3.3g, 10 mmol) was added into the reaction mixture. After stirring for 24 hr at 60 °C, the reaction mixture was cooled down to room temperature and poured into DI water (500mL), and extracted with ethyl acetate three times. The organic layer was washed with brine and DI water to remove NMP. The combined organic layer was dried over anhydrous $MgSO_4$ and filtered. After evaporating the solvent, the residue was purified by column chromatography on silica gel with a mixture of ethyl acetate and hexane (1:6, v:v) as an eluent to give the title compound as a dark purple solid. Yield: 0.35g (~10%).

^{1}H NMR (CDCl$_3$): 8.28(2H, d, J = 3.0 Hz), 7.62 (2H, d, J = 3.9 Hz), 7.19 -7.16 (2H, t, J = 4.5 Hz), 3.89-3.77 (2H, m), 1.90-1.70,(4H, m), 1.70-1.54 (4H, m), 1.50-1.10 (56H, m), 0.95-0.80(12H, m). (Figure 2.14)
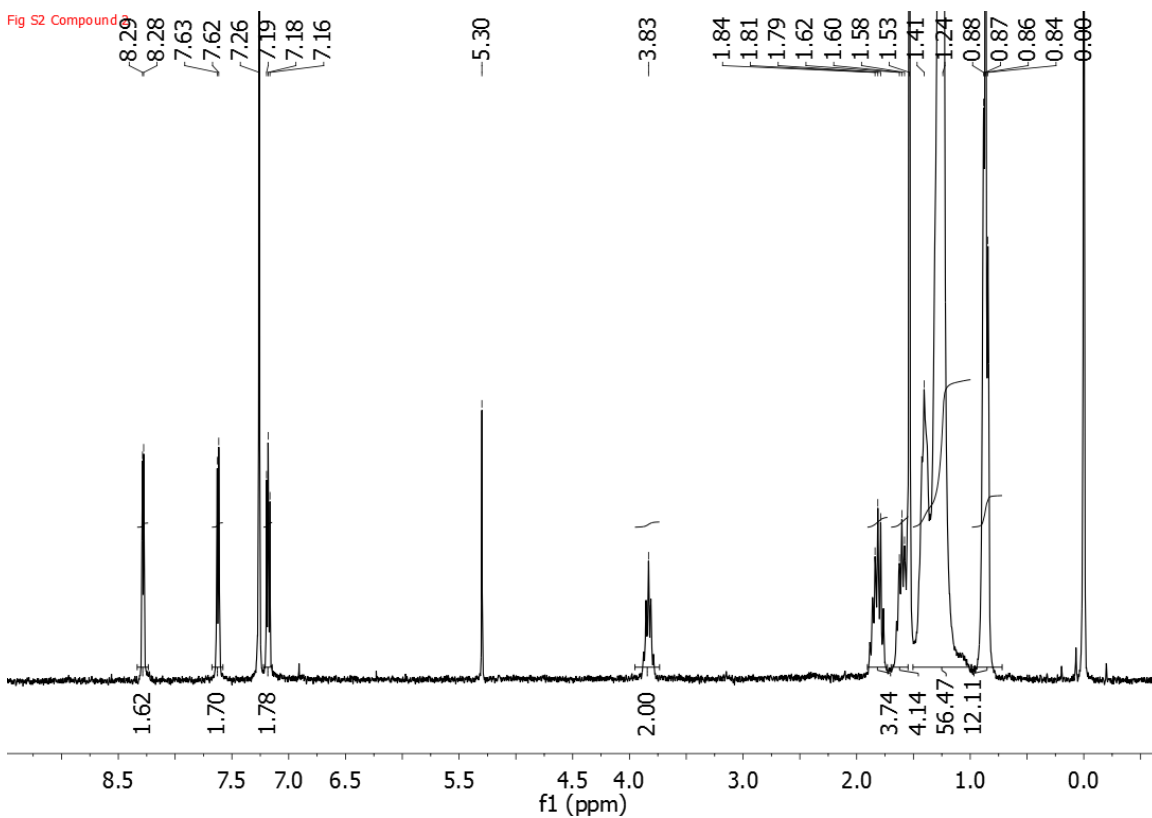
Figure 2.14 300 MHz ^{1}H NMR spectrum of 2,5-bis(2-octyldodecanoyl)-3,6-di(thiophen-2-yl)pyrrolo[3,4-c]pyrrole-1,4(2H,5H)-dione (2) in CDCl$_3$.

2.3.6 Synthesis of 3,6-bis(5-bromothiophen-2-yl)-2,5-bis(2-octyldodecanoyl)pyrrolo[3,4-c]pyrrole-1,4(2H,5H)-dione (3)
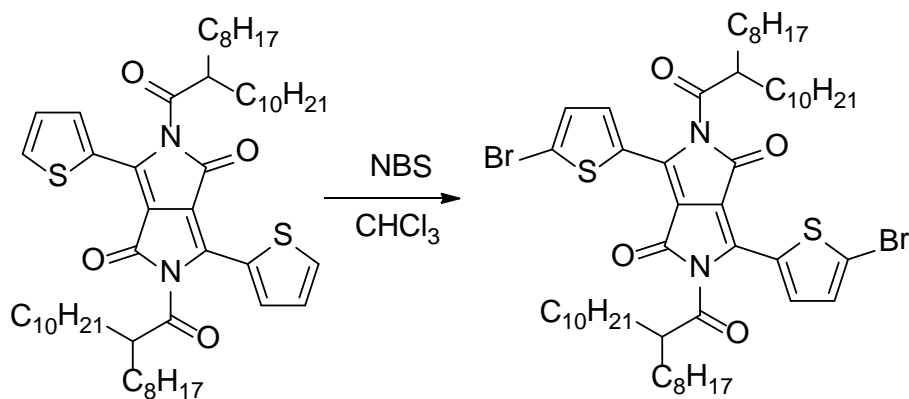
2,5-Bis(2-octyldodecanoyl)-3,6-di(thiophen-2-yl)pyrrolo[3,4-c]pyrrole-1,4(2H,5H)-dione

(2) (1.1g, 1.24 mmol) was dissolved in chloroform (50 mL) and NBS (0.441g, 2.48

mmol) was added. After stirring for 24 hr at room temperature in the absence of light, the

solvent in the reaction mixture was removed and the residue was purified with column

chromatography on silica gel using a mixture of dichloromethane and hexane (1:4, v:v) as

an eluent. A dark purple solid was obtained (0.85g, 65%).

^{1}H NMR (CDCl$_3$): 8.17(2H, d, J = 4.2 Hz), 7.14 (2H, d, J = 4.2 Hz), 3.88-3.76 (2H, m),

1.90-1.70 (4H, m), 1.70-1.54 (4H, m), 1.45-1.10(56H, m), 0.95-0.80(12H, t, J = 6.36 Hz).

(Figure 2.15)
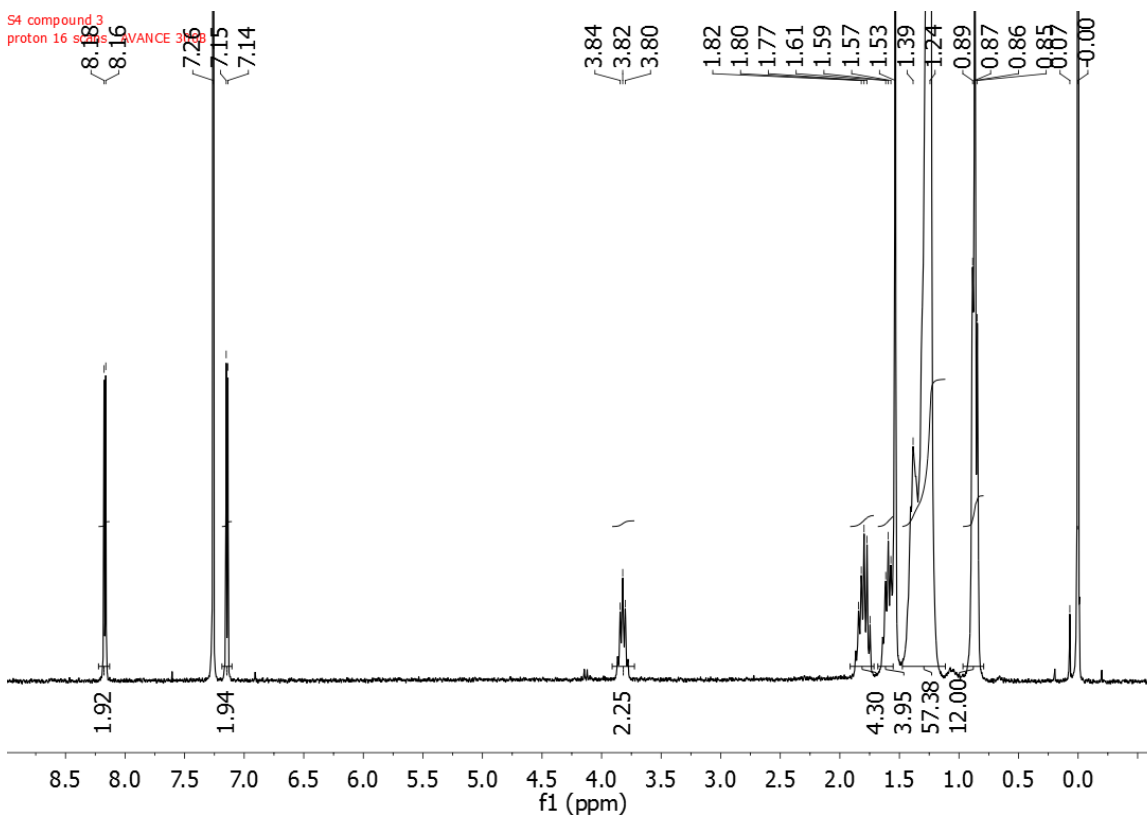
Figure 2.15 300 MHz ^{1}H NMR spectrum of 3,6-bis(5-bromothiophen-2-yl)-2,5-bis(2-octyldodecanoyl)pyrrolo[3,4-c]pyrrole-1,4(2H,5H)-dione (**3**) in CDCl$_3$.

2.3.7 5,5'-bis(trimethylstannyl)-2,2'-bithiophene [68]
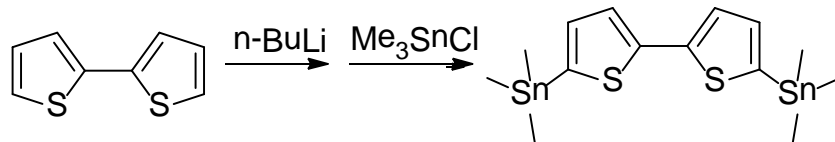
To a dry 100 ml Schenk flask containing 2,2'-bithiophene (2.1g, 6 mmol) and 50 ml of dry THF, a solution of n-butyl lithium in hexane (11mL, 2.5M, 27.5 mmol) was drop-wise added at -78 °C. The suspension was stirred at -78 °C for an additional 30 min. A solution of trimethyltin chloride in THF (30mL, 1M, 30mmol) was then added drop-wise. The solids reacted slowly and gave a pale yellow solution, which was then stirred for 4 h at -78 °C, then warmed to room temperature and poured into water. The organic layer was separated and dried over $MgSO_4$. After removal of the solvent by evaporation, the residue was recrystallized several times from hexane to obtain 1450 mg (49% yield) of 5,5'-bis (trimethylstannyl)-2,2'-bithiophene as light yellow crystals.

^{1}H NMR (CDCl$_3$): 7.26-7.25 (d, 2H), 7.07-7.06 (d, 2H), d 0.36 (s, 18H) (Figure 2.16)
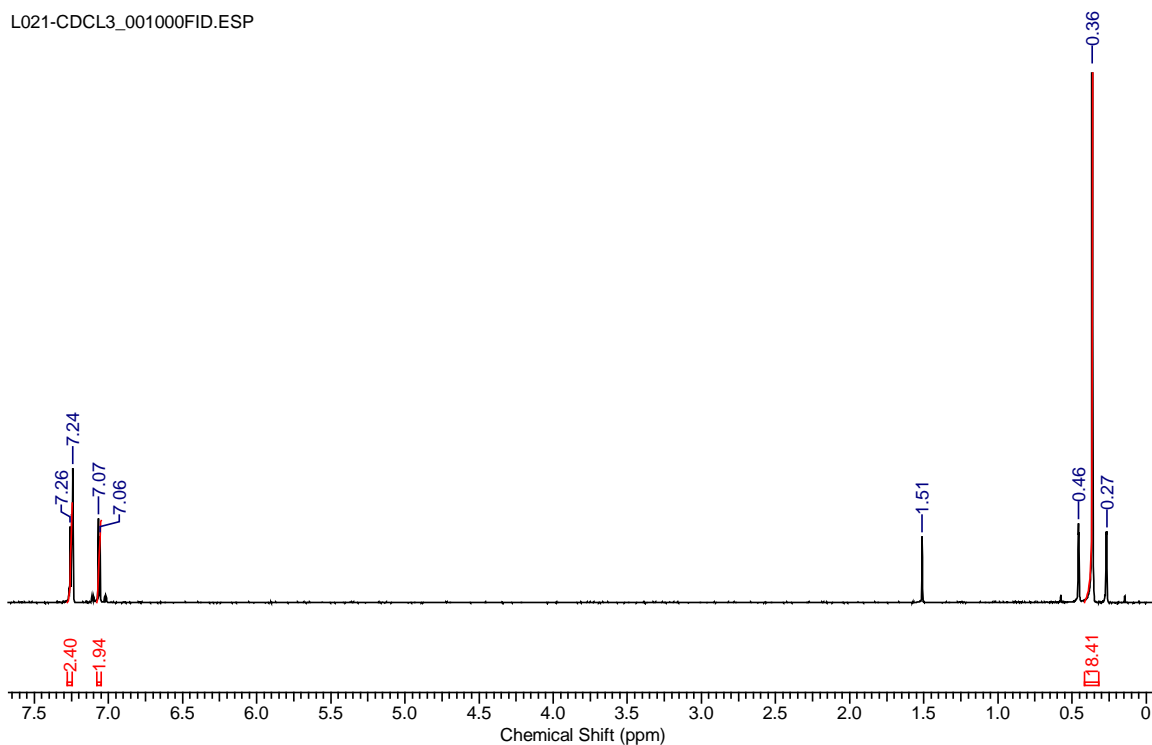
Figure 2.16 300 MHz ^{1}H NMR spectrum of 5,5'-bis(trimethylstannyl)-2,2'-bithiophene in CDCl$_3$.

2.3.8 Synthesis of poly(2,5-bis(2-octyldodecanoyl)-3,6-di(thiophen-2-yl)pyrrolo[3,4-*c*]pyrrole-1,4(2*H*,5*H*)-dione-alt-2,2'-bithiophene) (PDQT-tc)
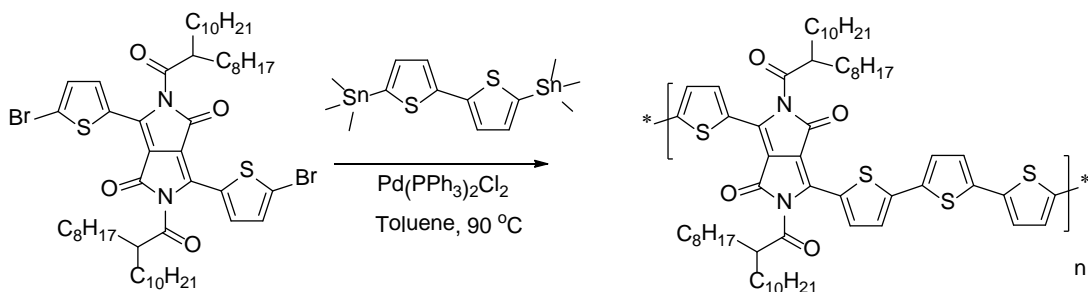
3,6-Bis(5-bromothiophen-2-yl)-2,5-bis(2-octyldodecanoyl)pyrrolo[3,4-*c*]pyrrole-

1,4(2*H*,5*H*)-dione (3) (0.2470 g, 0.236 mmol) and 5,5'-bis(trimethylstannyl)-bithiophene

(0. 1160 g, 0.236 mmol) were charged in a 50 mL flask. After degassing and refilling

with argon for 3 times, toluene (12 mL) and bis(triphenylphosphine)palladium(II)

39

dichloride (4.8 mg) were added and the reaction mixture was stirred at 80 °C for 1 hr, and then at 90 °C for 23 hr. Then 0.5 mL of bromobenzene was added and stirred at 90 °C for an additional 3 hr. The mixture was then poured into stirred methanol (200 mL). The solid was filtered off and further purified by Soxhlet extraction using acetone, hexane, before being dissolved with chloroform. A dark blue solid was obtained (227mg, 91.5%). GPC: M_n = 24,334; PDI = 3.90. ^{1}H NMR and GPC data were in Figure 2.17 and 2.18
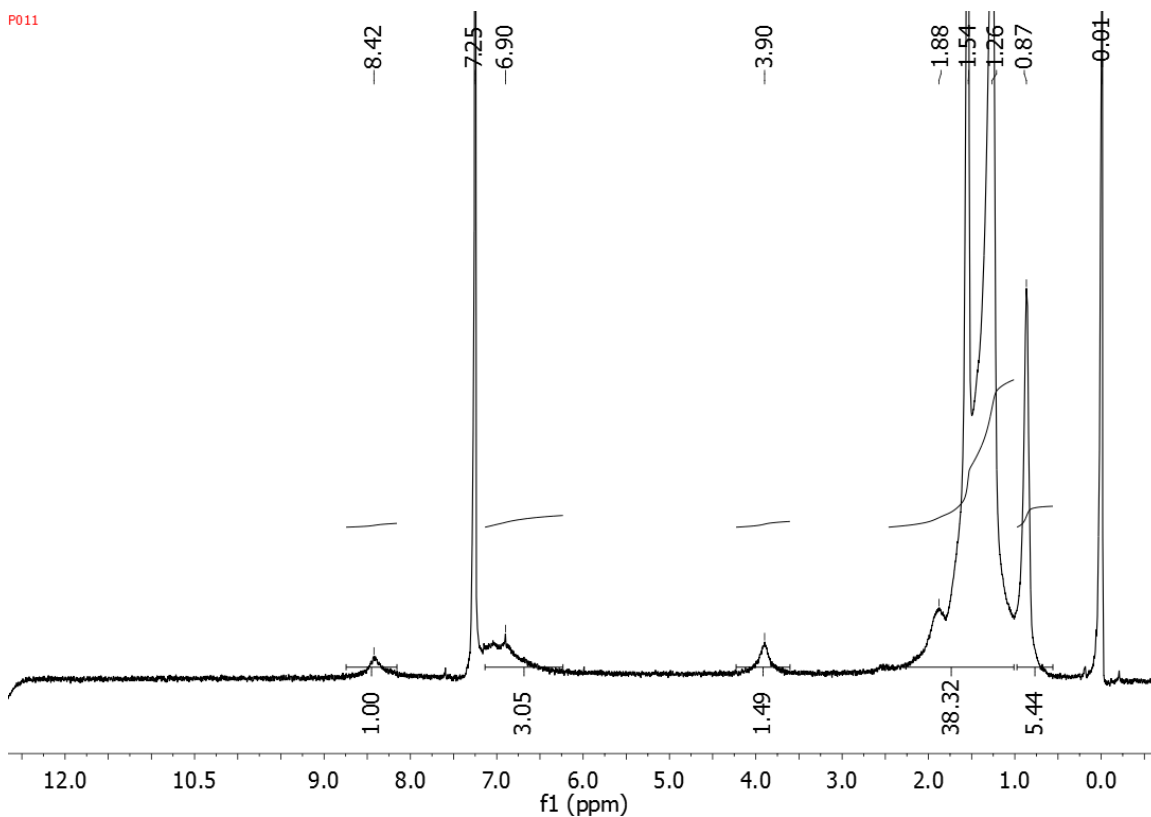
Figure 2.17 300 MHz ^{1}H NMR spectrum of **PDQT-tc** in CDCl$_3$.

SAMPLE INFORMATION

Sample Name:	P011	Acquired By:	PHOT
Sample Type:	Broad Unknown	Sample Set Name:	june 11
Vial:	2	Acq. Method Set:	Zhao April15
Injection #:	1	Processing Method:	ClBenzAug25_2011
Injection Volume:	50.00 ul	Channel Name:	410
Run Time:	40.0 Minutes	Proc. Chnl. Descr.:	
Date Acquired:	6/11/2012 10:50:11 AM EDT		
Date Processed:	6/11/2012 12:11:05 PM EDT		

GPC Results

	Dist Name	Mn	Mw	MP	Mz	Mz+1	Mv	Polydispersity	MW Marker 1	MW Marker 2
1		24344	95014	75323	431356	1514513		3.902967		
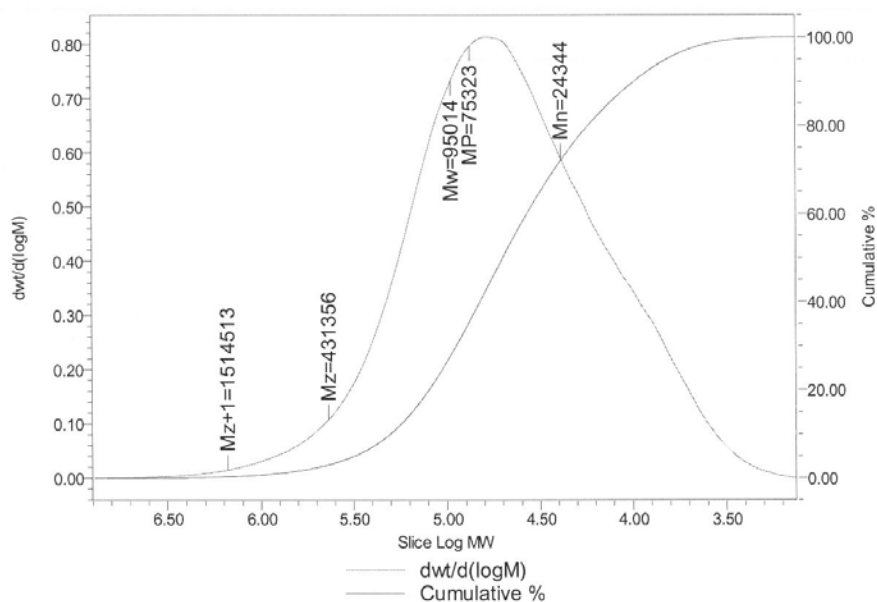
Figure 2.18 GPC profile of **PDQT-tc** using chlorobenzene as an eluent and polystyrene as standards at column temperature of 40 °C.

2.3.9 Fabrication and characterization of OTFT devices

A top contact, bottom-gate OTFT configuration was used to evaluate the polymer semiconductors. Heavily p-doped Si wafer with a thermally grown SiO_2 layer (~200 nm) having a capacitance of ~ 17 nF cm^{-2} was used as a substrate. In this configuration, the

41

conductive Si layer functions as the gate electrode and the SiO_2 layer as the dielectric. After cleaning sequentially with DI water, acetone, and isopropanol in an ultrasonic bath, the substrate was cleaned by O_2 plasma. Subsequently, the substrate was immersed in a dodecyltrichlorosilane (DTS) solution in toluene (10 mg mL^{-1}) at 70 °C for 20 min. The substrate was then washed with toluene, and dried under a nitrogen flow. A PDQT-tc solution in chloroform (5 mg ml^{-1}) was spin coated on the substrate at 1500 rpm for 60 s, resulting in a ~30-40 nm thick PDQT-tc thin film. A more concentrated PDQT-tc solution (10 mg mL^{-1}) was used to deposit a ~70 nm thick polymer film, which was annealed at 200 °C for 3 hr on a hotplate in a globe box, resulting in a PDQT-n film with a thickness of ~30 nm. Subsequently the source/drain electrode pairs were deposited on the polymer film by thermal evaporation of silver through a shadow mask. Finally the device was encapsulated by TiO_X [62] and annealed at 80 °C for 20 min under nitrogen. OTFT devices have a channel length (*L*) of 100 μm with a channel width (*W*) of 4 mm. The devices were characterized in air using an Agilent 4155C Semiconductor Analyzer. The field effect mobility was calculated according to the previously employed method.[27]

2.4 Conclusions

A novel polymer semiconductor was designed and synthesized with side chains thermally cleavable at a low temperature of 200 °C. The complete cleavage and removal of the insulating 2-octyldodecanoyl side chains were verified with TGA, FT-IR, and NMR data. The liberated N-H groups on the polymer backbone are expected to form intermolecular hydrogen bonds with the C=O groups on the neighbouring polymer chains to establish

three-dimensional charge transport networks. The resulting side chain-free conjugated polymer is proven an active p-type semiconductor material for OTFTs, exhibiting hole mobility of up to 0.078 $cm^2V^{-1}s^{-1}$. The resulting side chain-free polymer thin film is morphologically very stable, resistant to any solvents, and has a favourable band gap for light harvesting, which may also be a useful electron donor material for stable organic photovoltaics.

Chapter 3 DPP-based semiconducting polymer blends for OTFT application

3.1 Introduction

The side chain-free conjugated polymer reported in Chapter 2 is a p-type semiconductor material for OTFTs, exhibiting hole mobility of up to 0.078 $cm^2V^{-1}s^{-1}$ in amorphous phase in which the polymer backbones are rather twisted by inter-chain interactions. It would be a challenge to reorder the native polymer chain to give it a regular $\pi - \pi$ stacking structure.

Blending is an established strategy in polymer science to achieve specific structural and physical properties of the polymeric mixture. Insulating polymers, such as polystyrene (PS) and polymethylmethacrylate (PMMA), have been used to blend with P3HT.[80]

Blending of two conjugated polymers was first reported in photodiode applications in 1995, and enhanced performance.[74-76] In 2002, application of conjugated polymer blends was reported for light-emitting diodes.[77] Not only did the ratio of different conjugated polymers would affect the performance of devices due to tuned electronic properties, but also the fabrication process including the choice of solvent affected the morphology of polymer film and device performance. In 2006, Shikler et al reported that photovoltaic performance was linked to the polymer phase separation. They claimed that the de-mixing (or phase separation) is more complete in regions closer to the interface between the two phases and that carrier transport is easier in these regions than in the bulk. They also showed that the efficiency depended linearly on the length of the

44

interface between the phases.[78] In 2009, Hamilton and co-workers reported that the use of blends of poly(triarylamine) and 2,8-difluoro-5,11-bis(triethylsilylethynyl)anthradithiophene in solution process could reach charge carrier mobilities greater than 2 $cm^2V^{-1}s^{-1}$, which is higher than that of a single material. [79]

Here we have designed a series of experiments to blend the thermally decomposable polymer PDQT-tc with polystyrene or PDQT to overcome the problem of reduced crystallinity we encountered with pure PDQT-tc (see Chapter 2). As a result, the hole transport mobilities as high as 3.08 $cm^2V^{-1}s^{-1}$ were obtained for the PDQT-tc/PDQT blends, which is significantly higher than the individual PDQT-tc or PDQT.

3.2 Results and Discussion

Conjugated polymer blends were evaluated in bottom-gate, bottom-contact OTFT devices, with a device structure shown in Figure 3.1. A heavily n-doped silicon wafer with a ~200-nm thermally grown SiO_2 layer was used as the substrate. The conductive silicon functions as the gate electrode and the SiO_2 layer as the dielectric with a capacitance of ~14nF/cm^2. The SiO_2 layer was pre-deposited by a Au electrode using photolithography method. Then the substrate was modified with dodecyltrichlorosilane (DTS) prior to use. A conjugated polymer blend solution in tetrachloroethane (TCE) was spin coated on the substrate at 1500 rpm for 60 s to form a ~60-70nm polymer thin film, which was subjected to thermal annealing at 150 °C for 15min or 200 °C in a glove box. OTFT devices have a channel width (*W*) of 1 mm and a channel length (*L*) of 30 µm. All devices were measured in air and in the dark.

Figure 3.1 Bottom gate, bottom contact structure of OTFT devices

In Table 3.1, PDQT-tc blended with an insulating polymer were shown to give OFET performance with hole transport mobility of 0.11 and 0.094 $cm^2V^{-1}s^{-1}$ at 150 °C and 200 °C annealing, respectively. These results are similar to that of the pure PDQT-tc polymer film described in Chapter 2, which are 0.096 and 0.078 $cm^2V^{-1}s^{-1}$ at 150 °C and 200 °C annealing, respectively. This could be explained by the phenomenon of vertical phase separation reported previously. [80,81] AFM images of the blend thin films before and after thermal decomposition clearly showed evidence of phase separation in the PDQT-n produced at 200 C ° formed phase separation with grain sizes of 10-100 nm. The dark grains are most likely the PDQT-n, while the light matrix is the PS phase. Apparently the PDQT-n phase is unfavorably separated by the insulating PS phase, which is not beneficial for charge hopping between the PDQT-n grains. Our results indicate that blending PDQT-tc with an insulating polymer such as PS could not improve the charge transport performance of PDQT-tc after thermal decomposition.

Table 3.1 OFTT electronic properties of PDQT-tc mixed with insulator polymers

	150°C 15min annealing PS:PDQT-tc 1:1	200°C annealing without pressure PS:PDQT-tc 1:1
Mobility $(cm^2V^{-1}S^{-1})$	0.11	0.094
On/Off	3.2×10^4	1.1×10^5
V_T (V)	7.7	-23.3
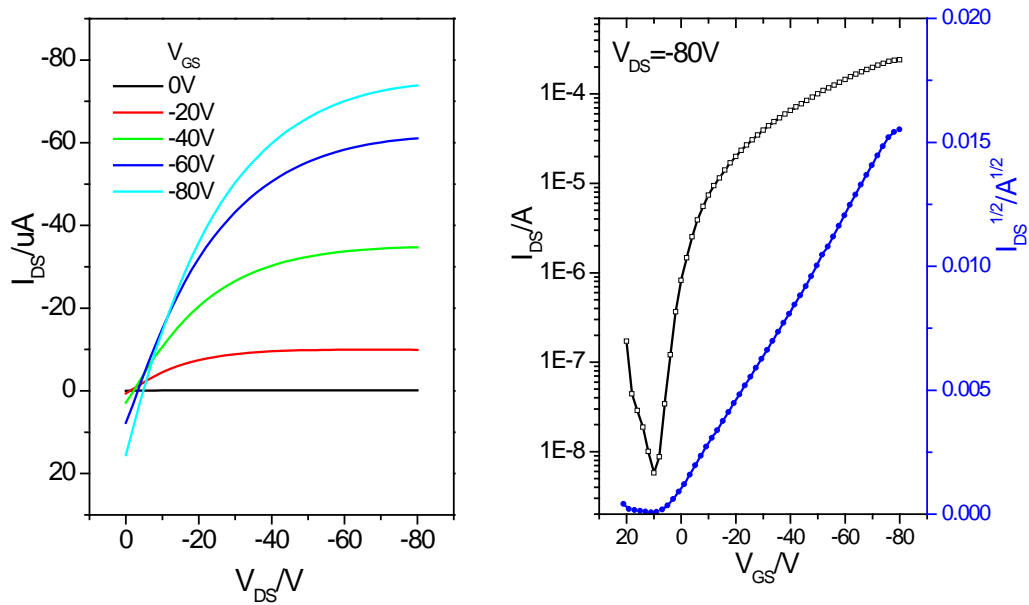
Figure 3.2 Output and transfer curves (left) and transfer curve (right) of an OTFT device with a PDQT-tc and PS blends with a ratio of 1:1 (m:m) thin film annealed at 150 °C for 15 min. Device dimensions: channel width (*W*) =1 mm; channel length (*L*) =30 µm.
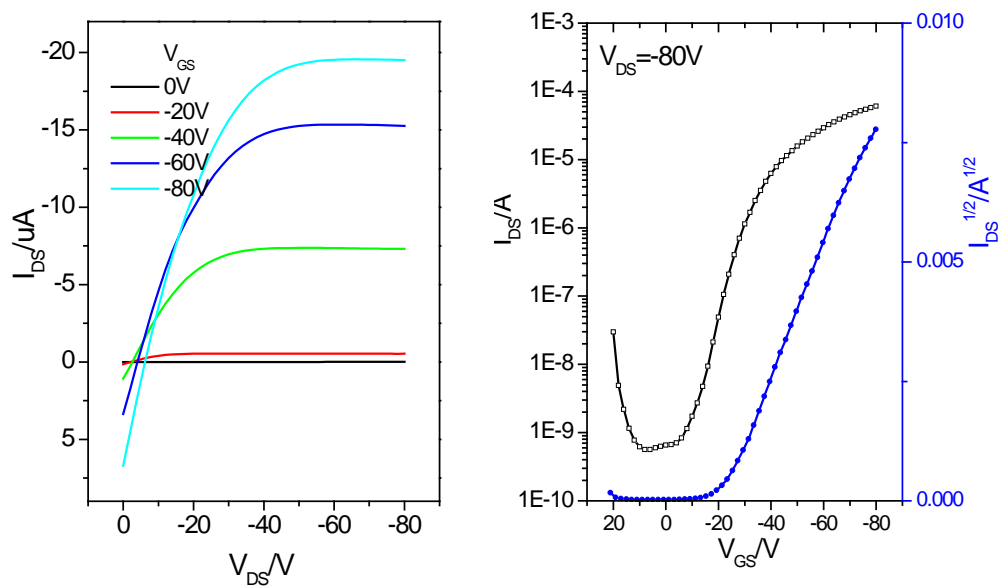
Figure 3.3 Output and transfer curves (left) and transfer curve (right) of an OTFT device with a PDQT-tc and PS blends with a ratio of 1:1 (m:m) thin film annealed at 200 °C for 3hr. Device dimensions: channel width (W) =1 mm; channel length (L) =30 µm.
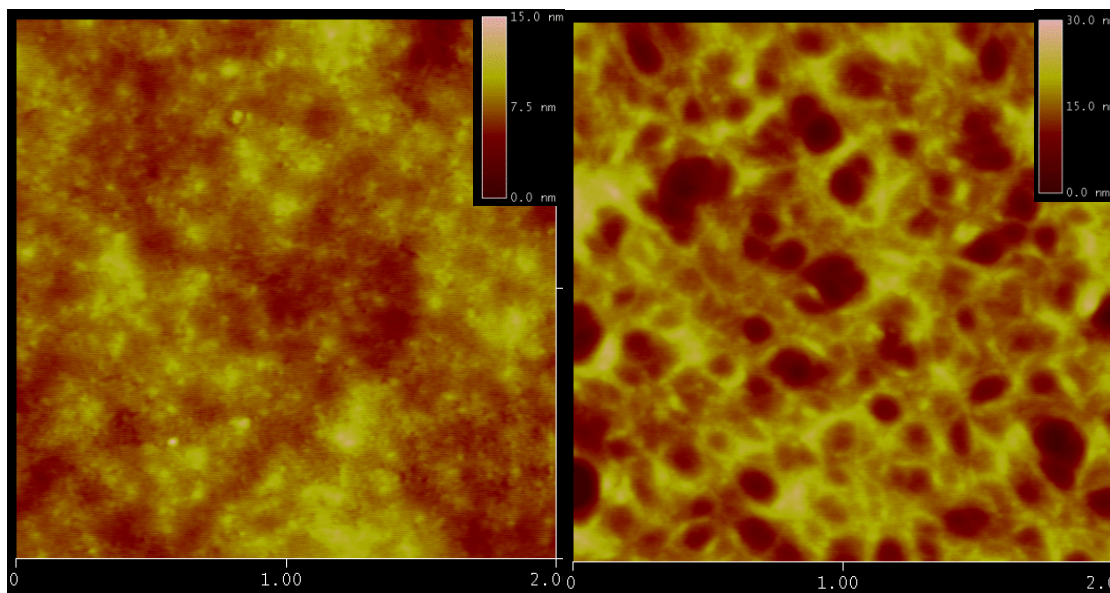
Figure 3.4 AFM images (2 µm × 2µm) of PDQT-tc / PS blend thin films annealed at 150 °C (left) for 15min and 200 °C (right) for 3hr in nitrogen.

From the knowledge learned from the PDQT-tc/PS blends, we decided to use PDQT, a semiconducting polymer, instead of the insulating PS, to blend with PDQT-tc. We expected that the matrix formed by the semiconducting PDQT would function as a bridge to connect the PDQT-n grains formed after thermal decomposition.
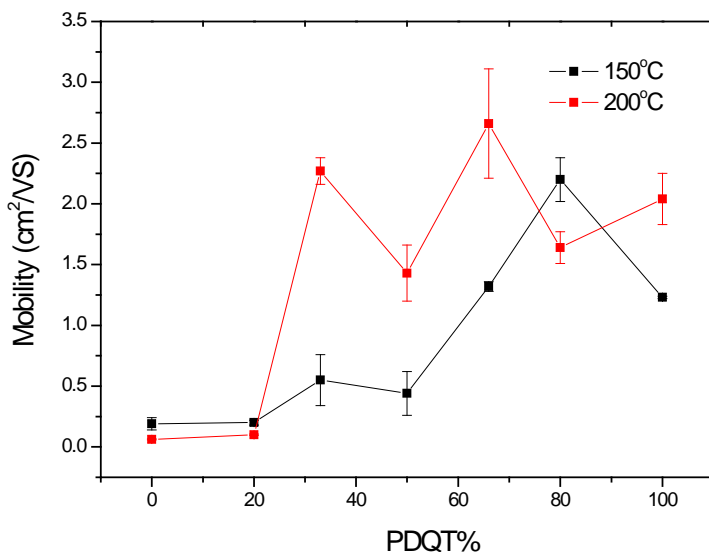
Figure 3.5 Average hole transport mobility measured from saturation region as a function of the PDQT content (wt%) in the blends.

The polymer film was evaluated with a bottom gate, bottom contact structure over a range of polymer blends in TCE. The devices were annealed at 150 °C for 15min or 200 °C for 3hr. Finally, the devices were encapsulated by PMMA with a thickness of 500nm. The hole transport mobilities were measured with the method introduced in Chapter 1 to yield the results shown in Figure 3.5.

For the 150 °C- annealed sample, the hole transport mobility calculated from the saturation region of the pure PDQT is up to 1.24 $cm^2V^{-1}s^{-1}$. For the PDQT/PDQT-tc blend (4:1), it is interesting to observe that the mobility can be as high as 2.42 $cm^2V^{-1}s^{-1}$. The reason for this improvement can be ascribed to the large crystal grains of the PDQT phase with the assistance of PDQT-tc, as observed in Figure 3.6 a and b.
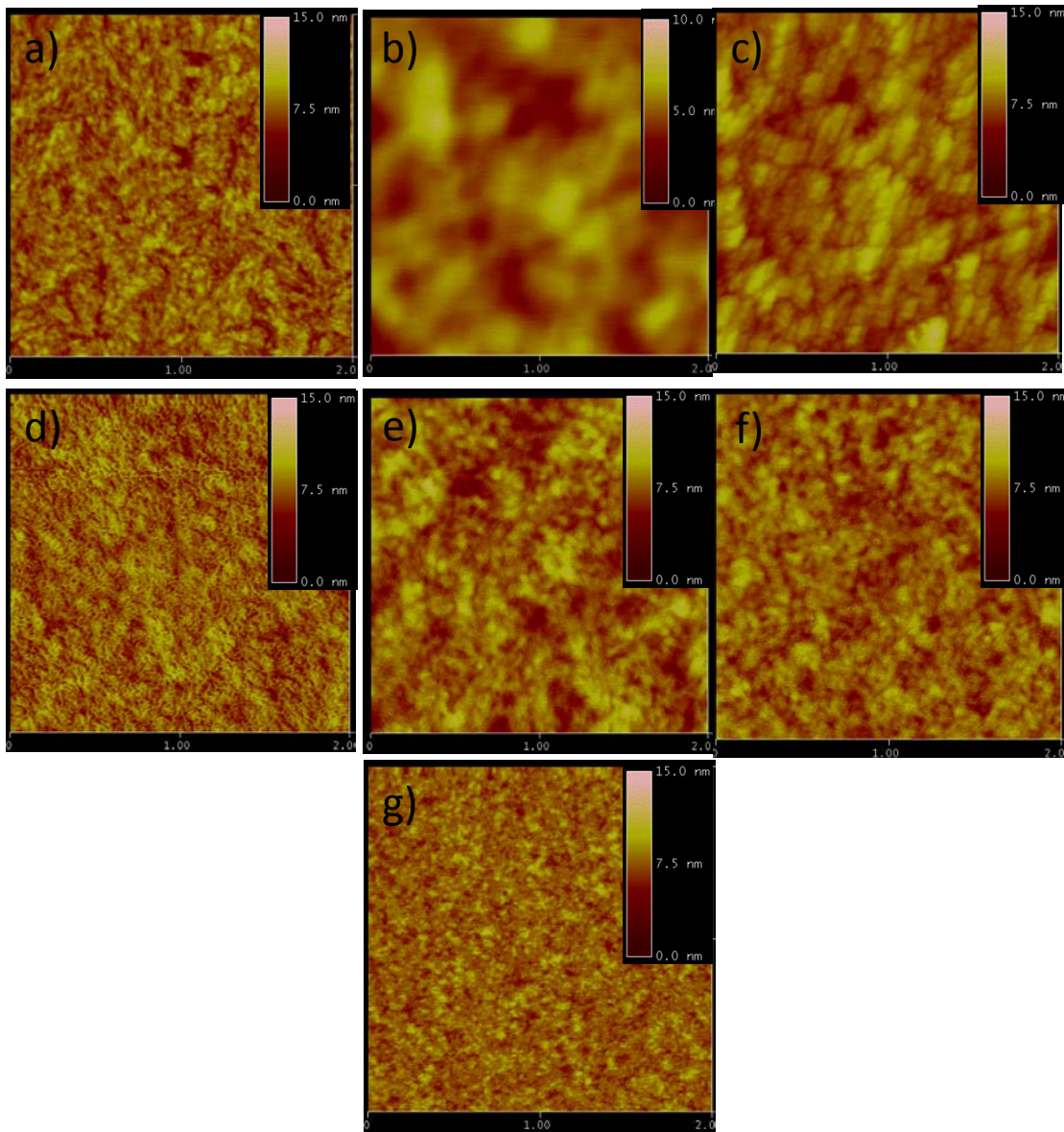
Figure 3.6 2µm×2µm AFM image of PDQT/PDQT-tc blends film annealed at 150 °C with PDQT/PDQT-tc blends ratio: a) 1:0, b) 4:1, c) 2:1, d) 1:1, e)1:2, f) 1:4, g) 0:1.

When the amount of PDQT-tc was increased, the mobility decreased gradually. At a PDQT/PDQT-tc ratio of 1:4 (20 wt-%), the mobility value is close to that of the pure PDQT-tc.

When the film was annealed at 200°C for 3 hr, the change of mobility versus the the PDQT content (wt-%) in the blends is impressive, and the blends of PDQT/PDQT-tc with a ratio of 2:1 and 1:2 gave a higher average mobility of 2.66 and 2.27 $cm^2V^{-1}s^{-1}$ than the mobility of 2.04 $cm^2V^{-1}s^{-1}$ of the pure PDQT film. The AFM images in Figure 3.7 b and c showed small particles in the film. From the component of the blends, we can propose the bigger particles are the crystal grains of PDQT, and the smaller particles are grains of side-chain free PDQT-n. Figure 3.7b shows the blend film formed at a ratio of 4:1 of PDQT/PDQT-tc. The average mobility is 1.64 $cm^2V^{-1}s^{-1}$, which is lower than the mobility of 2.04 $cm^2V^{-1}s^{-1}$ of pure PDQT polymer. This could be attributed to the phase separation of the two polymers since the grains of the PDQT phase are larger than those in the pure PDQT film. However, the distance between the PDQT grains also become longer, which is responsible for the reduced mobility. For the PDQT/PDQT-tc blend with a ratio of 2:1, a highest mobility value of 3.08 (with an average of 2.66 $cm^2V^{-1}s^{-1}$) was achieved. This could also be linked to phase separation. In Figure 3.7c, many small PDQT-n particles surround the large PDQT grains and filled the gaps between the large particles.
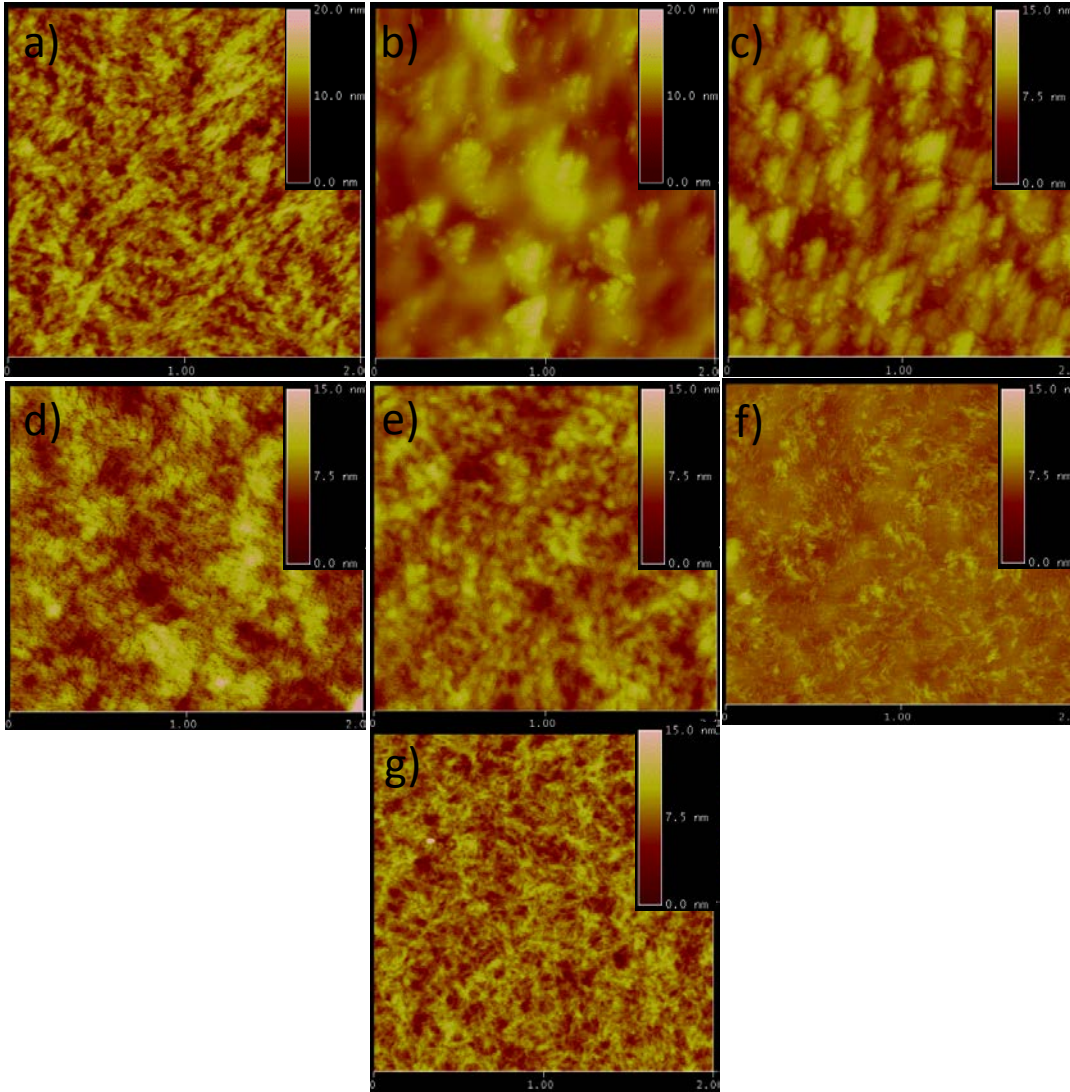
Figure 3.7 2µm×2µm AFM image of PDQT/PDQT-tc blends film annealed at 200°C with PDQT/PDQT-tc blends ratio: a) 1:0, b) 4:1, c) 2:1, d) 1:1, e) 1:2, f) 1:4, g) 0:1.

The blend with 1:1 ratio gave an average mobility of 1.43 $cm^2V^{-1}s^{-1}$. From the AFM image in Figure 3.7d the grains are smaller. The blend with a ratio of 1:2 showed again a higher average mobility value of 2.27 $cm^2V^{-1}s^{-1}$. Figure 3.7e showed that this film consists of tightly packed nanograins.

The output and transfer characteristics are listed in Figures 3.8 to 3.21.
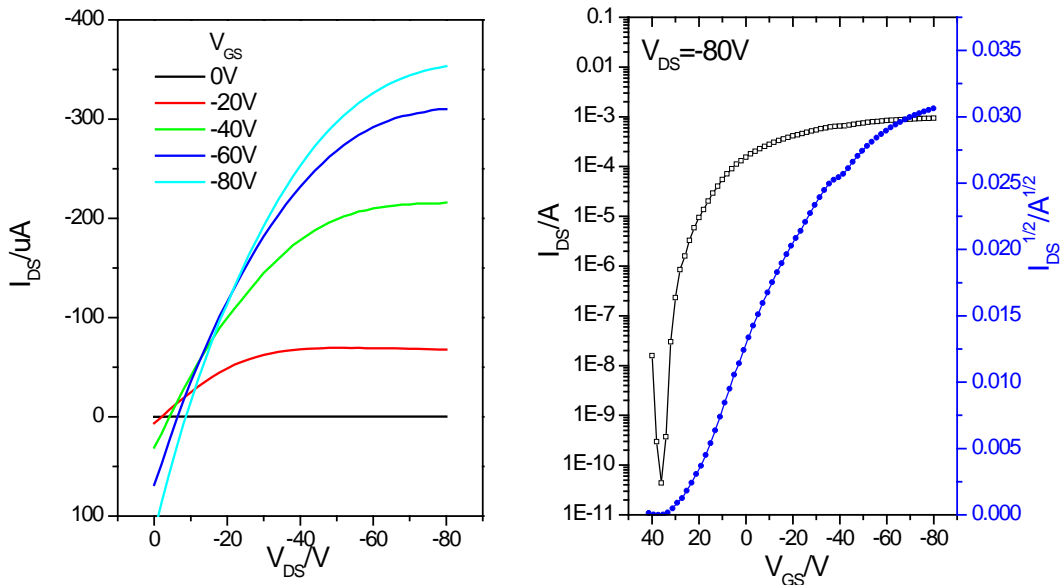
Figure 3.8 Output and transfer curves (left) and transfer curve (right) of an OTFT device with a PDQT thin film annealed at 150 °C for 15min. Device dimensions: channel width (*W*) =1 mm; channel length (*L*) =30 µm.
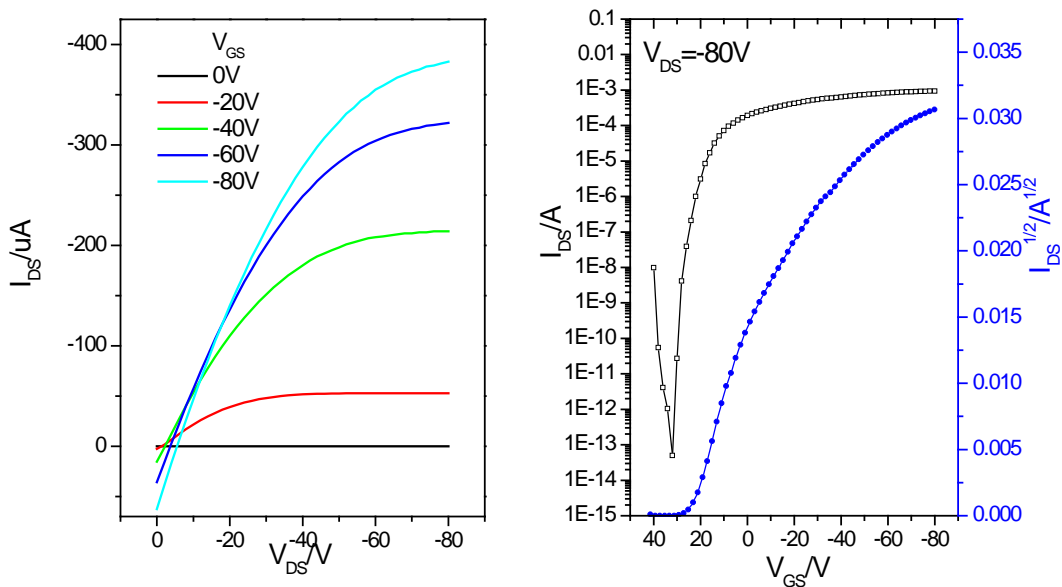
Figure 3.9 Output and transfer curves (left) and transfer curve (right) of an OTFT device with a PDQT thin film annealed at 200 °C for 15min. Device dimensions: channel width (*W*) =1 mm; channel length (*L*) =30 µm.
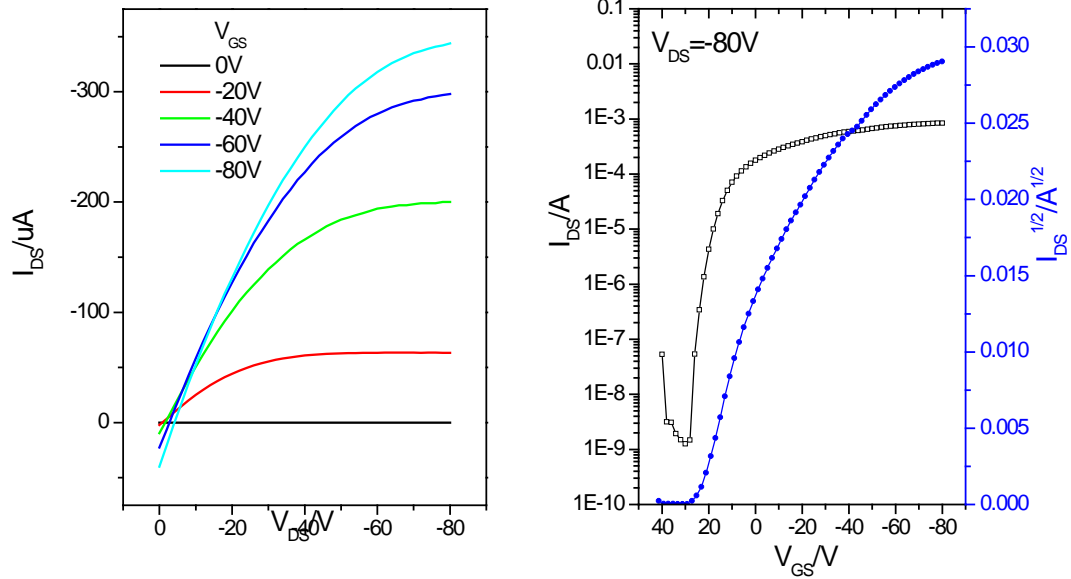
Figure 3.10 Output and transfer curves (left) and transfer curve (right) of an OTFT device with a PDQT and PDQT-tc blends with a ratio of 4:1 thin film annealed at 150 °C for 15min. Device dimensions: channel width (*W*) =1 mm; channel length (*L*) =30 µm.
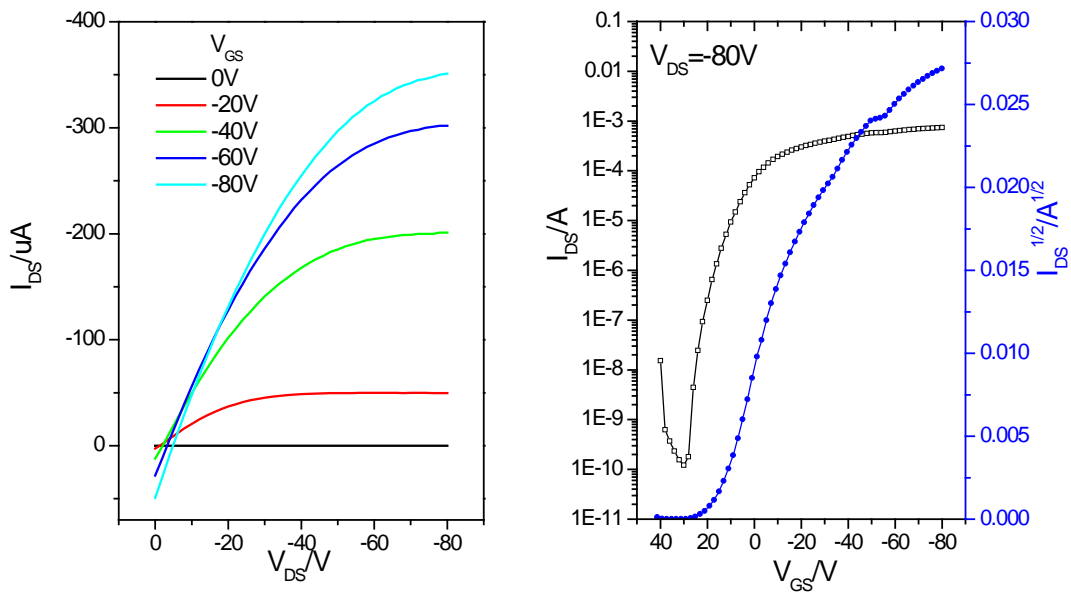
Figure 3.11 Output and transfer curves (left) and transfer curve (right) of an OTFT device with a PDQT and PDQT-tc blends with a ratio of 4:1 thin film annealed at 200 °C for 3hr. Device dimensions: channel width (*W*) =1 mm; channel length (*L*) =30 µm.
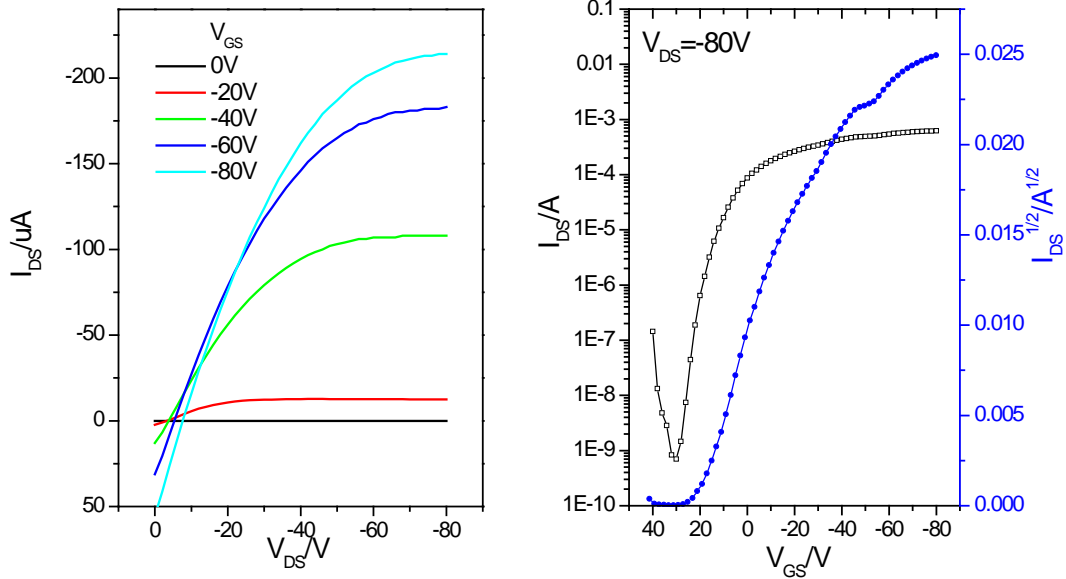
Figure 3.12 Output and transfer curves (left) and transfer curve (right) of an OTFT device with a PDQT and PDQT-tc blends with a ratio of 2:1 thin film annealed at 150 °C for 15min. Device dimensions: channel width (W) =1 mm; channel length (L) =30 µm.
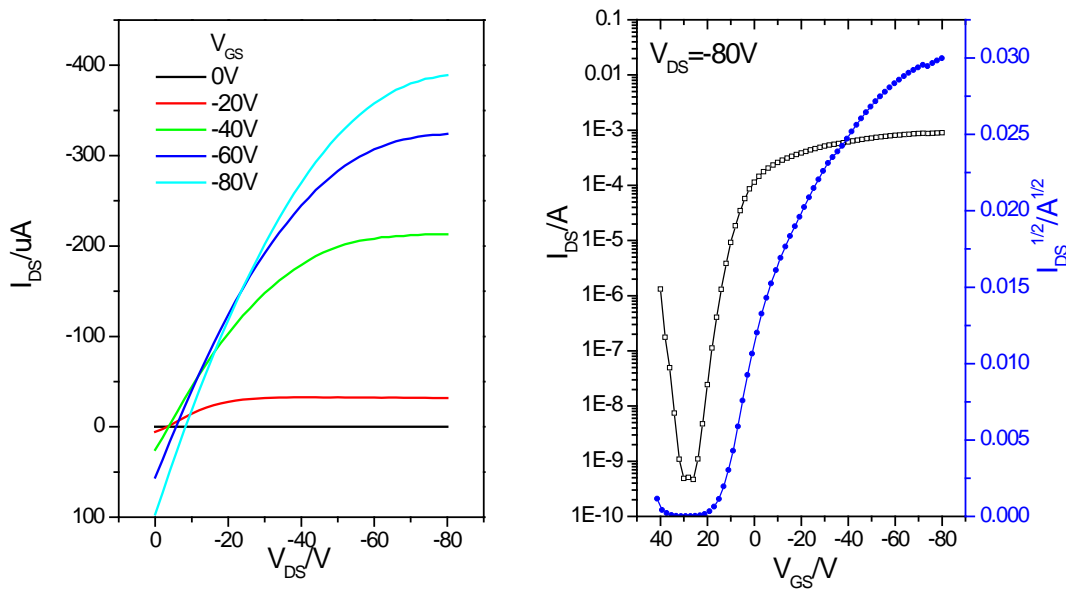
Figure 3.13 Output and transfer curves (left) and transfer curve (right) of an OTFT device with a PDQT and PDQT-tc blends with a ratio of 2:1 thin film annealed at 200 °C for 3hr. Device dimensions: channel width (W) =1 mm; channel length (L) =30 µm.
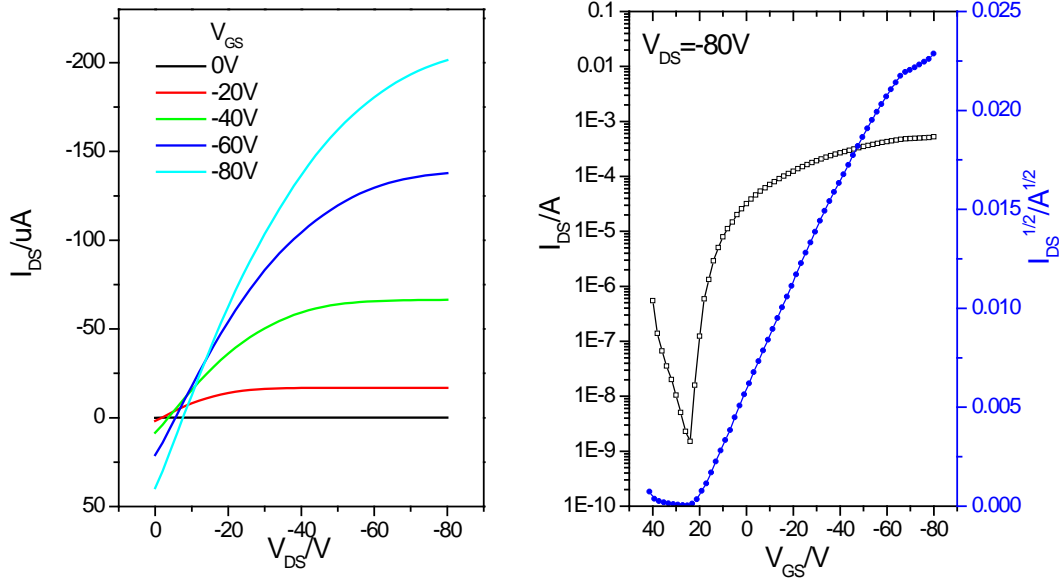
Figure 3.14 Output and transfer curves (left) and transfer curve (right) of an OTFT device with a PDQT and PDQT-tc blends with a ratio of 1:1 thin film annealed at 150 °C for 15min. Device dimensions: channel width (*W*) =1 mm; channel length (*L*) =30 µm.
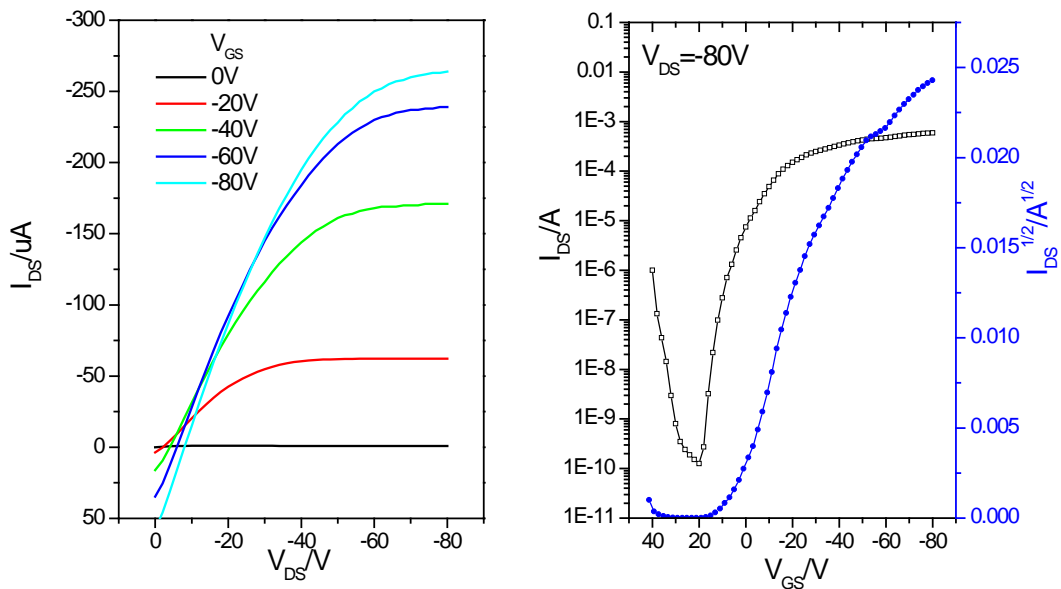
Figure 3.15 Output and transfer curves (left) and transfer curve (right) of an OTFT device with a PDQT and PDQT-tc blends with a ratio of 1:1 thin film annealed at 200 °C for 3hr. Device dimensions: channel width (*W*) =1 mm; channel length (*L*) =30 µm.
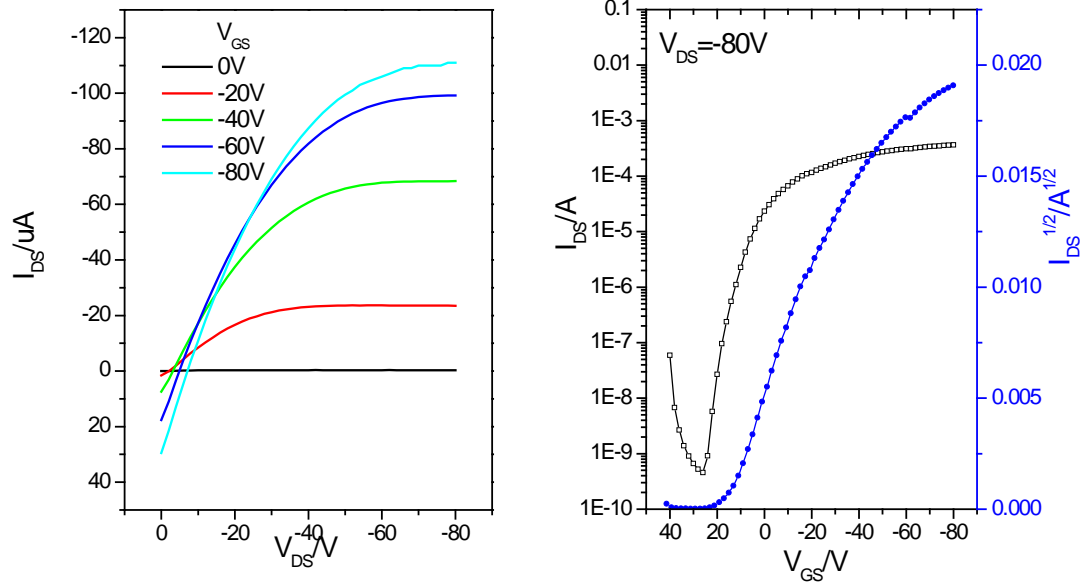
Figure 3.16 Output and transfer curves (left) and transfer curve (right) of an OTFT device with a PDQT and PDQT-tc blends with a ratio of 1:2 thin film annealed at 150 °C for 15min. Device dimensions: channel width (*W*) =1 mm; channel length (*L*) =30 µm.
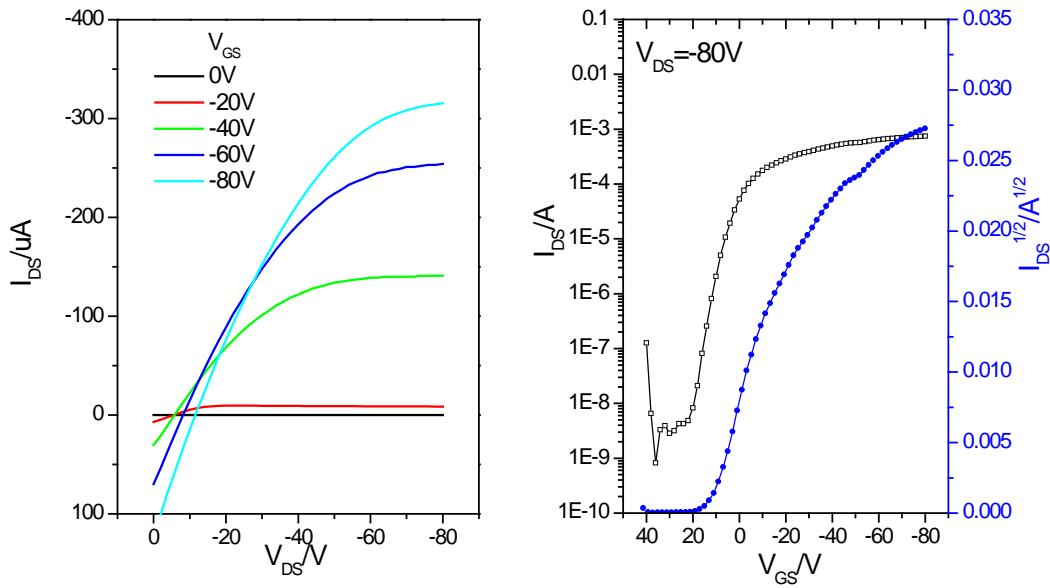
Figure 3.17 Output and transfer curves (left) and transfer curve (right) of an OTFT device with a PDQT and PDQT-tc blends with a ratio of 1:2 thin film annealed at 200 °C for 3hr. Device dimensions: channel width (*W*) =1 mm; channel length (*L*) =30 µm.
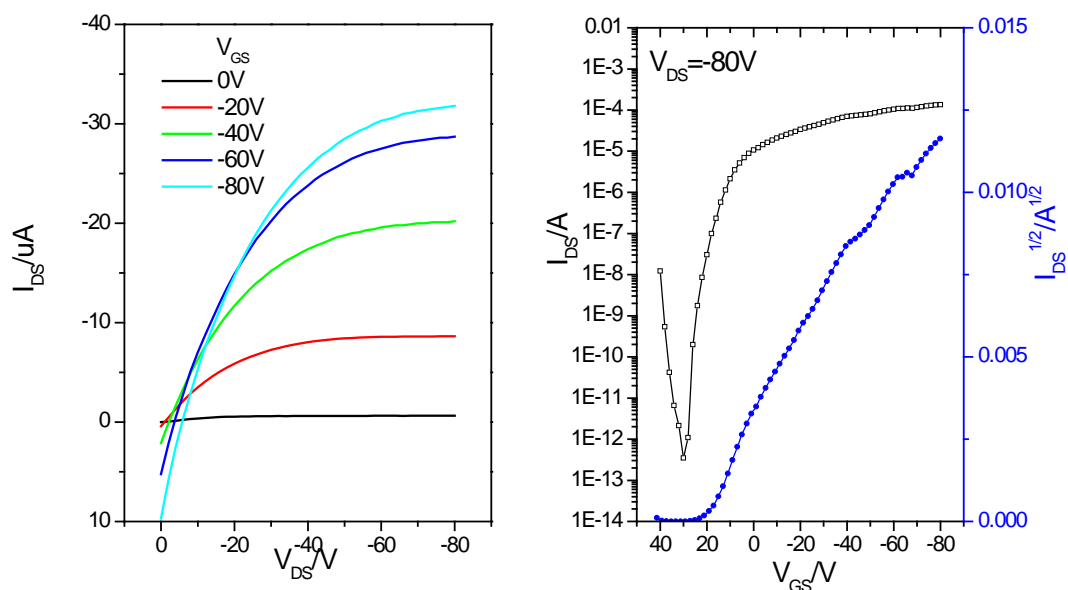
Figure 3.18 Output and transfer curves (left) and transfer curve (right) of an OTFT device with a PDQT and PDQT-tc blends with a ratio of 1:4 thin film annealed at 150 °C for 15min. Device dimensions: channel width (W) =1 mm; channel length (L) =30 µm.
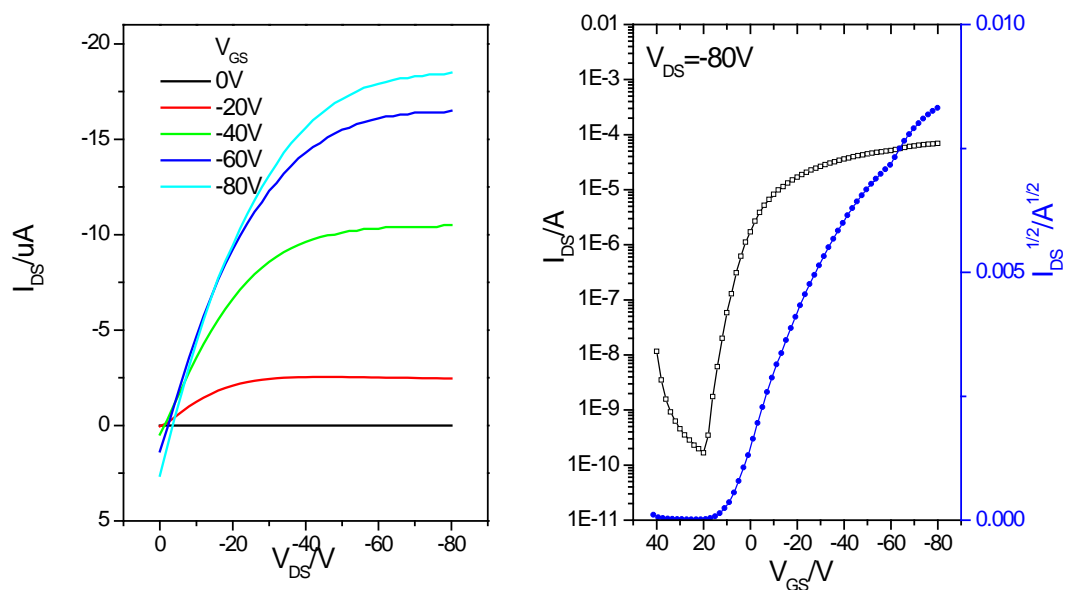
Figure 3.19 Output and transfer curves (left) and transfer curve (right) of an OTFT device with a PDQT and PDQT-tc blends with a ratio of 1:4 thin film annealed at 200 °C for 3hr. Device dimensions: channel width (W) =1 mm; channel length (L) =30 µm.
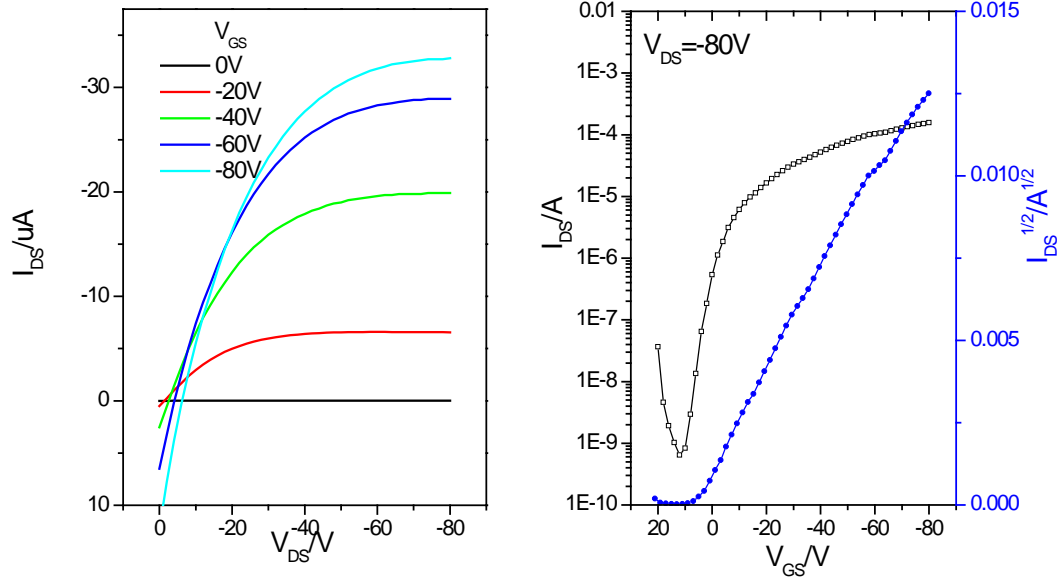
Figure 3.20 Output and transfer curves (left) and transfer curve (right) of an OTFT device with a PDQT-tc thin film annealed at 150 °C for 15min. Device dimensions: channel width (*W*) =1 mm; channel length (*L*) =30 µm.
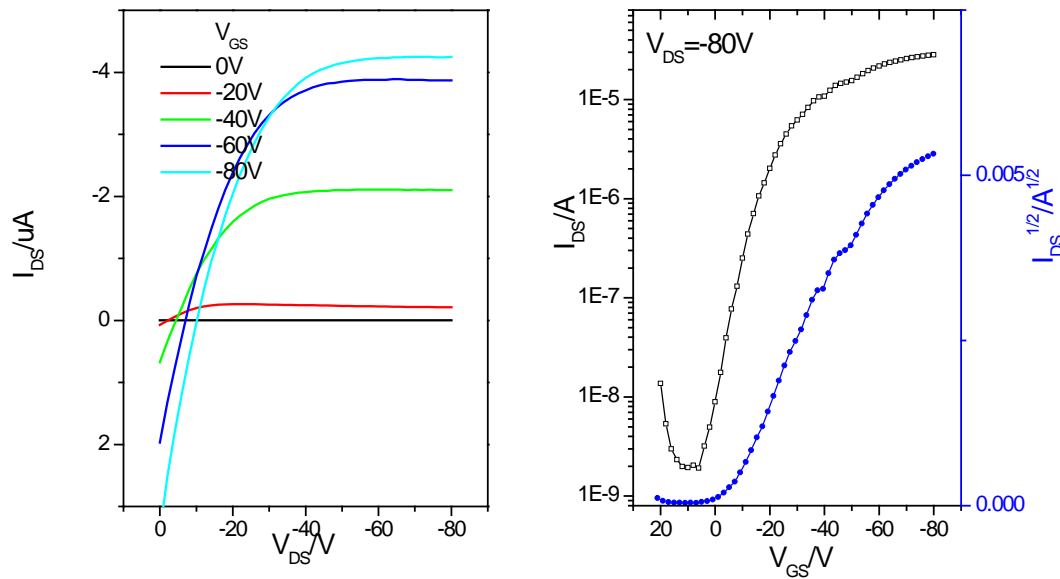
Figure 3.21 Output and transfer curves (left) and transfer curve (right) of an OTFT device with a PDQT-tc thin film annealed at 200 °C for 3hr. Device dimensions: channel width (*W*) =1 mm; channel length (*L*) =30 µm.

3.3 Experimental

3.3.1 Fabrication of substrate
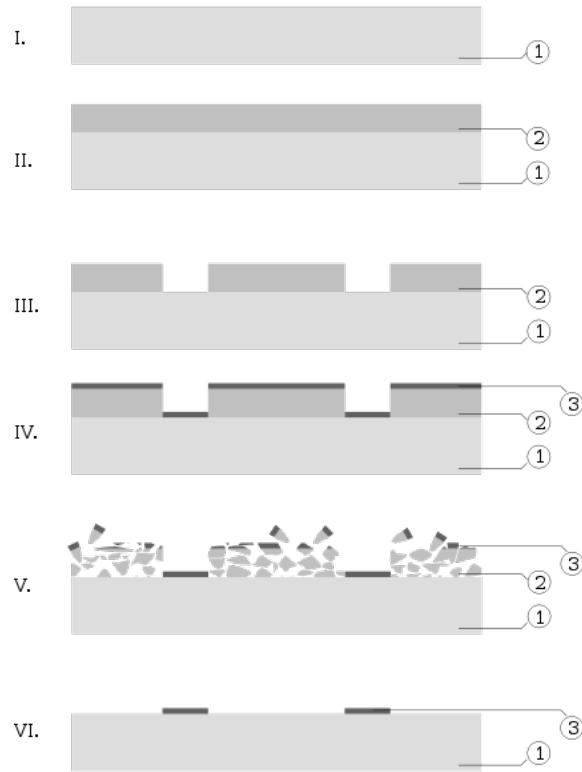
Figure 3.22 Process of fabrication of OTFT electrode pattern.[73]

The device substrate patterns were fabricated as follows:

The silicon wafer with SiO_2 dielectric layer substrate was cleaned and covered by PR AZ3312 with a thickness of 1um, and exposed for 4.0s. Then the substrate was developed in AZ300MF developer for15s. Finally, a 3nm layer of Cr and 37nm layer of Au were deposited step by step. Following this step, the photoresist was removed using a stripper. The finished substrate is shown in Figure 3.23.
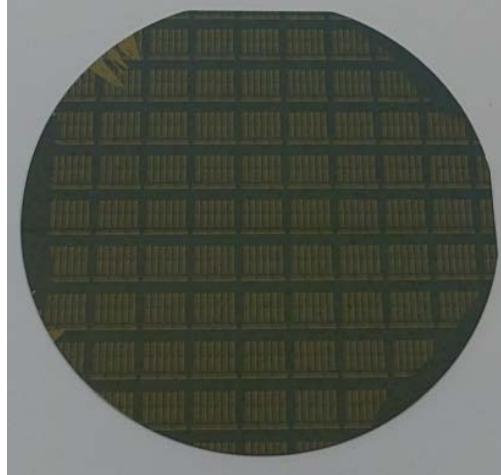
Figure 3.23 Picture of OTFT electrodes pattern on a silicon wafer with a size of 4 inches

3.3.2 Fabrication and characterization of OTFT devices

Conjugated polymer blends were evaluated in bottom-gate, bottom-contact OTFT devices. Heavily n-doped silicon wafer with a ~200-nm thermally grown SiO_2 layer was used as the substrate. The conductive silicon functions as the gate electrode and the SiO_2 layer as the dielectric with a capacitance of ~14nF/cm^2. The SiO_2 layer was pre-deposited with Au electrode with photolithography method. Then the substrate was modified with dodecyltrichlorosilane (DTS) prior to use. A conjugated polymer blends solution in TCE was spin coated on the substrate at 1500 rpm for 60 s to form a ~60-70nm polymer thin film, which was subjected to thermal annealing at 150°C for 15min or 200°C for 3hr in a glove box. After that, the devices were encapsulated by PMMA with a thickness of 500nm. OTFT devices have a channel width (*W*) of 1 mm and a channel length (*L*) of 30 µm. All the devices were characterized in air using an Agilent 4155C Semiconductor Analyzer. The field effect mobility was calculated according to the previously employed method introduced in Chapter 1.

3.4 Conclusion

In this chapter, the technique of blending organic semiconductors for solution processing is employed in the fabrication of high performance OTFTs, and a charge transport mobility of up to 3.08 $cm^2V^{-1}s^{-1}$ was obtained with a high performance conjugated polymer PDQT and a novel thermally decomposable conjugated polymer PDQT-tc. Impressively, the performance is higher than the individual pure PDQT and PDQT-tc, which is explained by the favoured phase separation during the thermal decomposition of PDQT-tc. Our results demonstrated that blending two conjugated polymers, particularly for conjugated polymers with thermocleavable side chains, is a very promising technique to enhance of the performance the polymer semiconductors.

Chapter 4 Organic thin-film field-effect transistors with hole injection layer between electrode and active layer

4.1 Introduction

Polymer semiconductors have attracted much attention in recent years as active materials in organic thin film transistors (OTFTs).[34-38] OTFTs have potential applications in RFID, flexible displays, electronic paper, organic memory and photo voltaic devices due to the low cost in large area processing and low temperature in fabrication.[6-9] The HOMO level for p-type carrier transport should be below -5 eV and LUMO level for n-type transport should be below -4 eV. Most metal electrodes have a work function above -5eV. Consequently contact resistance would exist because of the mismatch of the low work function of electrode and the low HOMO level of the polymer semiconductor. Since the contact resistance between the electrodes and the semiconductor layer is critical to OTFT device performance, good contact would improve the device significantly.[69-72] Therefore, not only better organic materials, such as D-A structure polymer, need to be developed, but also device fabrication process need to be optimized.

Metal oxides, especially transition metal oxides, are low-cost, non-toxic, transparent, and can be easily processed for device fabrication. More importantly, they span a range of work functions and energy levels, which enable them to overcome the energy barriers to eliminate contact resistance between the semiconductor and the electrode material for efficient charge injection.

Here we investigate the fabrication of an OTFT device with a MoO_3 buffer layer between the silver electrode and conjugated polymer active layer to improve the device performance. In this work, we use 3,6-di(furan-2-yl)pyrrolo[3,4-*c*]pyrrole-1,4(2*H*,5*H*)-dione and bithiophene copolymer (PDBFBT), reported by our group, [59] which showed typical p-type semiconductor performance in OTFTs. As shown in Figure 4.1, Ag and Au are not ideal electrode materials for the hole injection from electrode to the PDBFBT active layer, which would result in a serious contact resistance.[59] On the other hand, MoO_3 has a valence band at -5.4 eV, which matches the HOMO level of PDBFBT polymer perfectly. Therefore we used MoO_3 as a buffer layer between the Ag electrode and the semiconductor layer.
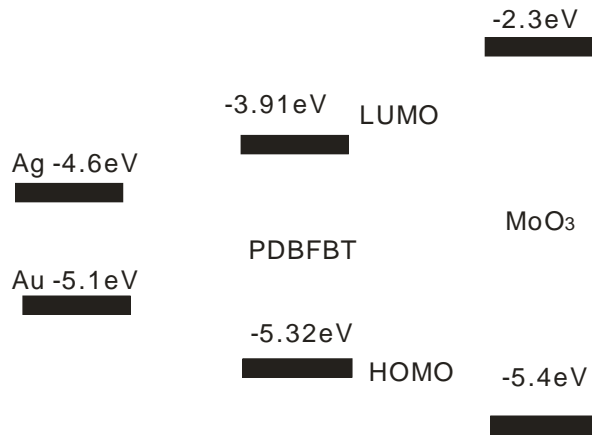
Figure 4.1 Energy level diagrams of PDBFBT, MoO_3, Ag and Au

4.2 Results and Discussion
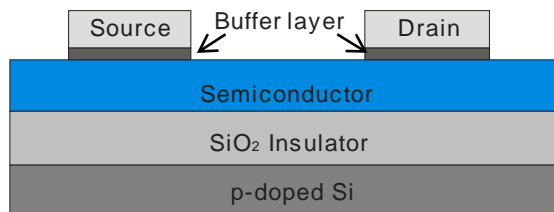
Figure 4.2 The OTFT device structure with a bottom gate and top contact structure and buffer layer between electrode and semiconductor layer
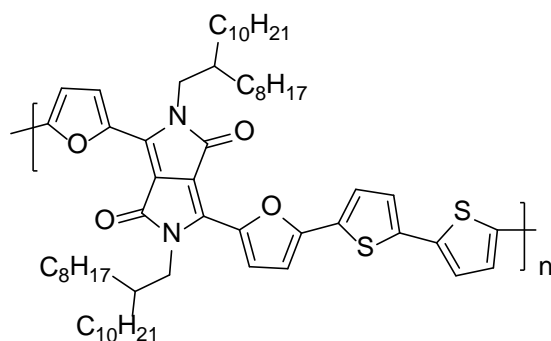
Figure 4.3 Chemical structure of PDBFBT

PDBFBT was tested in bottom-gate, top-contact OTFT devices. Heavily p-doped silicon wafer with a ~200-nm thermally grown SiO_2 layer was used as the substrate. As before the conductive silicon functions as the gate electrode and the SiO_2 layer as the dielectric. And the substrate was cleaned with acetone, IPA and DI water; the SiO_2 layer was then modified with dodecyltrichlorosilane (DTS) prior to use. A PDBFBT solution in chloroform was spin-coated on the silicon substrate at 1500 rpm for 60 s to form a ~30-40-nm polymer thin film. The devices were thermally annealed at 180 °C. Then silver was deposited on the polymer film by thermal evaporation through a shadow mask to form OTFT device with a channel width (W) of 4 mm and a channel length (L) of 150 µm.

We compared several different electrodes, including Ag without buffer layer, Ag with 10nm of MoO_3 buffer layer, Ag with mixed deposited buffer layer of 5nm of NPB and 5nm of MoO_3, and Ag with mixed deposited buffer layer of 5nm of Ag and 5nm of MoO_3.
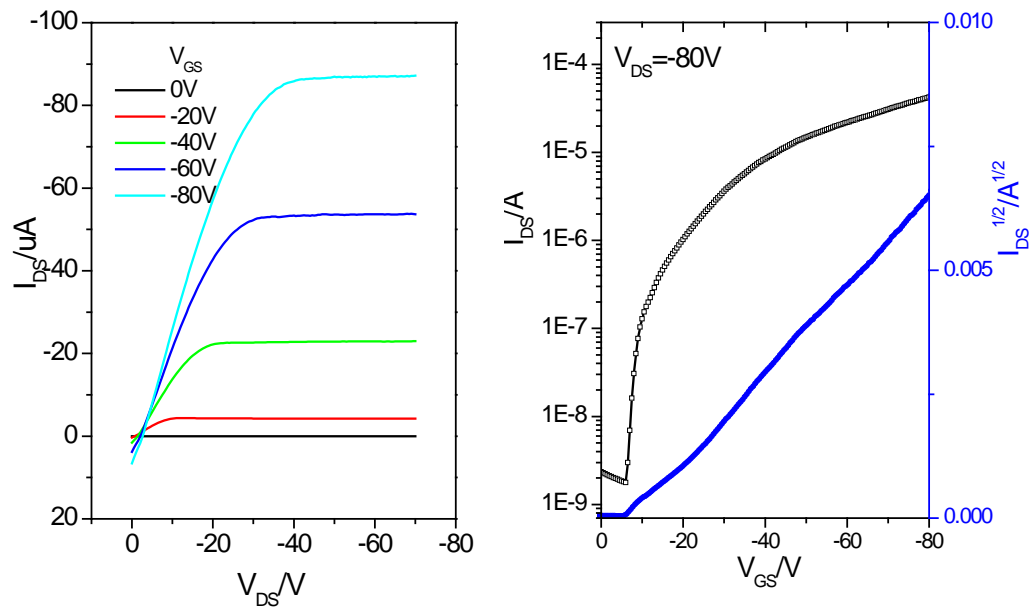
Figure 4.4 Output and transfer curves of an OTFT device with a PDBFBT thin film and 100nm of Ag electrode annealed at 180 °C for 15 min
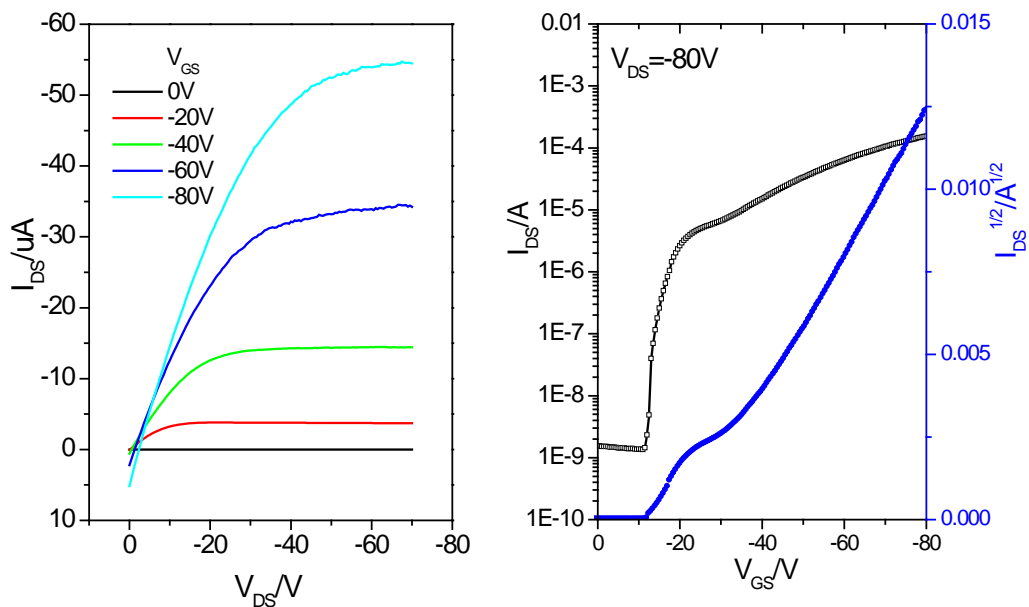
Figure 4.5 Output and transfer curves of an OTFT device with a PDBFBT thin film and Ag electrode with 10nm of MoO_3 buffer layer annealed at 180 °C for 15 min
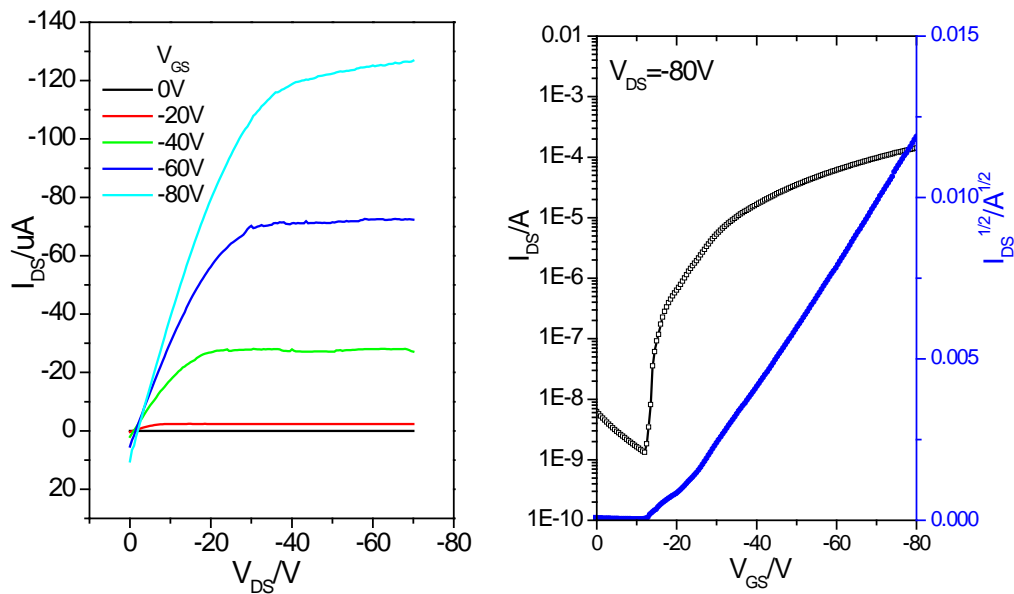
Figure 4.6 Output and transfer curves of an OTFT device with a PDBFBT thin film and Ag electrode with mixed buffer layer of 5nm of Ag and 5nm of MoO_3 annealed at 180 °C for 15 min

Table 4.1 Electrical parameters of the OTFTs in this study

Electrode	Ion/Ioff	V_T/V	Mobility/ $cm^2V^{-1}s^{-1}$
Ag (100nm)	5.0E+04	-15	0.12
Ag/MoO$_3$ (10nm)	9.8E+04	-23	0.21
Ag/mixed Ag-MoO$_3$	2.3 E+04	-20	0.19
Ag/ mixed NPB-MoO$_3$	3.0E+5	-20	0.33

All the devices were fabricated in nitrogen filled glove box, while they were tested in air.

Table 4.1 lists the mobility of devices, and the value of mobility is smaller than the value

we reported. These results are reasonable because the data we got in the paper [59] were

collected in nitrogen filled environment. The DPP base polymer is very sensitive to

moisture, and the mobility obtained in air could be 1 order smaller than that obtained

without moisture.

Firstly, comparing values of mobility with different electrode, we found the mobility with

MoO$_3$ buffer layer between semiconductor layer and Ag electrode was higher than that

without MoO$_3$ layer, 0.20 to 0.12 $cm^2V^{-1}s^{-1}$. This could be because of the improvement of

hole injection by MoO$_3$. The use of 10nm of MoO$_3$ buffer layer and 10nm of mixed layer

of MoO$_3$ and Ag showed similar results, 0.21 compared to 0.19 $cm^2V^{-1}s^{-1}$. Due to the

diffusion of Ag in thermal evaporation, Ag could penetrate the 10nm of layer of MoO$_3$,

and the difference between MoO$_3$ and mixed layer of Ag and MoO$_3$ would be the

thickness of layer of MoO$_3$. This would be reasonable because the effect of hole injection

with a thickness of MoO$_3$ from 8 to 30nm has previously shown to be constant. [72]

To improve the efficiency of hole injection, a hole transfer material NPB was introduced

to the buffer layer in Figure 4.7. This yielded the highest value measured in air i.e., 0.33

$cm^2V^{-1}s^{-1}$. As a hole transport layer in LED study, NPB has good performance in organic

electric application; the high mobility we obtained maybe due to the low conductivity of MoO$_3$. Also NPB layer made the buffer layer more conductive.
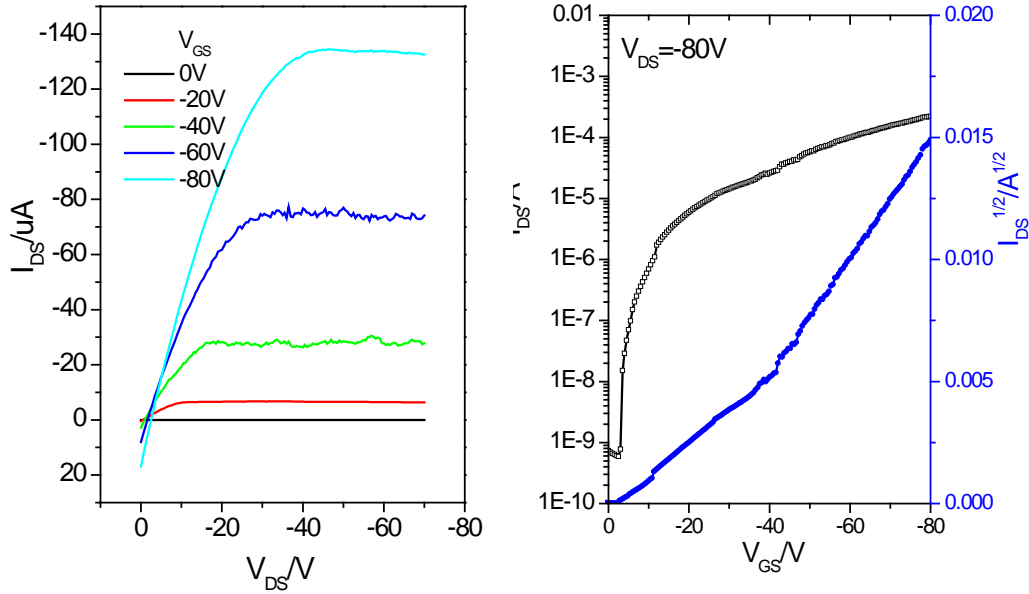
Figure 4.7 Output and transfer curves of an OTFT device with a PDBFBT thin film and Ag electrode with mixed buffer layer of 5nm of NPB and 5nm of MoO$_3$ annealed at 180 °C for 15 min

4.3 Experimental

4.3.1 Fabrication and characterization of OTFT devices

PDBFBT was evaluated in bottom-gate, top-contact OTFT devices. Heavily p-doped silicon wafer with a ~200-nm thermally grown SiO$_2$ layer having a capacitance of ~ 17 nF cm^{-2} was used as the substrate, where the conductive silicon functions as the gate electrode and the SiO$_2$ layer as the dielectric. The substrate was cleaned by Acetone, IPA and DI water, while the SiO$_2$ layer was modified with dodecyltrichlorosilane (DTS) prior to use. A PDBFBT solution in chloroform was spin-coated on the silicon substrate at 1500 rpm for 60 s to form a ~30-40-nm polymer thin film, which was subjected to

thermal annealing at 180 °C. Then electrode was deposited on polymer film by thermal evaporation of silver through a shadow mask to form OTFT devices with a channel width (W) of 4 mm and a channel length (L) of 150 µm.

Four different electrodes were deposited on the polymer surface

1. 100nm of Ag

2. 10nm of MoO_3, 100nm of Ag sequentially

3. 10nm of mixed evaporation (1:1) Ag and MoO_3, 100nm of Ag sequentially

4. 10nm of mixed evaporation (1:1) NPB and MoO_3, 100nm of Ag step-by-step

The devices were characterized in air using an Agilent 4155C Semiconductor Analyzer. The field effect mobility was calculated according to the previously employed method introduced in Chapter 1.

4.4 Conclusion

The OTFTs with MoO_3 as a hole injection layer between the silver electrodes and the polymer semiconductor film layer were fabricated through thermal evaporation. Compared with OTFTs without the metal oxide, the field-effect mobility was significantly improved.

Then NPB was mixed with the MoO_3 layer to improve the effect of hole injection, the mobility. Therefore, using a hole injection layer including a metal oxide with matching energy level or organic hole transport layer is an effective way to improve the performance of OTFTs, making the device suitable for organic electric applications.

Chapter 5. Conlusions and future work

5.1 Thermally decomposable semiconductor polymer

A novel polymer semiconductor with side chains thermally cleavable at a low temperature of 200 °C was synthesized. The complete cleavage and removal of the insulating 2-octyldodecanoyl side chains were verified with TGA, FT-IR, and NMR data. The liberated N-H groups on the polymer backbone are expected to form intermolecular hydrogen bonding with the C=O groups on the neighbouring polymer chains to establish three-dimensional charge transport networks. The resulting side chain-free conjugated polymer is proven an active p-type semiconductor material for OTFTs, exhibiting a hole mobility of up to 0.078 $cm^2V^{-1}s^{-1}$.

5.2 Organic transistors based on semiconducting blends

The technique of blending organic polymers for solution processing is employed in the fabrication of high performance OTFTs with a charge carrier mobility of up to 3.08 $cm^2V^{-1}s^{-1}$ based on a high performance conjugated polymer PDQT and a novel thermally decomposable conjugated polymer PDQT-tc. The performance of the semiconductor polymer blends is higher than each pure homo conjugated polymer. Thus, this opens up the great potential to use multicomponent systems in OFET and organic electronics fabrication.

5.3 Hole injection layer with metal oxide and organic hole transfer material

The OTFTs with MoO_3 or NPB as a hole injection layer between the silver electrodes and the polymer semiconductor film layer were fabricated through thermal evaporation. Compared with OTFTs without the metal oxide, the field-effect mobility was significantly improved. Therefore, using a hole injection layer including metal oxide with matching energy level or organic hole transport layer is an effective way to improve the performance of OTFTs, making the device suitable for organic electric applications.

5.4 Future Work

The thermally decomposable polymer combined by other donor and acceptor units will be synthesized and analysed. The native thin film is morphologically very stable, resistant to any solvents, and has a favourable band gap for light harvesting, which may also be utilized for stable organic photovoltaics. For the effective intrinsic mobility of side-chain free conjugated polymer, this kind of conjugated polymer could be utilized to improve the whole performance of organic electric devices by the technique of blending conjugated polymers.

Metal oxides with high work functions, e.g., MoO_3, WO_3, and TiO_2 will be used as a buffer layer to align the metal work function with the HOMO of the polymer. And other organic hole transport or electron transport layers will be evaluated to determine if an ambipolar material can be used for unipolar application.

References

1. Transistor In *American Heritage Dictionary*, 3rd Ed ed.; Boston: Houghton Mifflin, 1992

2. J. Chelikowski, "Introduction: Silicon in all its Forms", Silicon: evolution and future of a technology (Editors: P. Siffert, E. F. Krimmel), p.1, Springer, 2004 ISBN 3-540-40546-1.

3. J. E. Lilienfeld, US Pat. US1745175

4. Kahng, Dawon, U. S. Pat. US3102230

5. H. Koezuka, A. Tsumura, and T. Ando, *Synthetic Metals*, **1987**, 18, 699–704

6. M. O. Ahmed, C.Wang, P. Keg, W. Pisula, Y. M. Lam, B. S. Ong, S. C. Z. Ng, Z.-K. Chen, and S. G. J. Mhaisalkar, *Mater.Chem.* **2009**, 19, 3449–3456.

7. H.H. Fong, V. A. Pozdin, A. Amassian, G. G. Malliaras, D. Smiglies, M. He, S. Gasper, F. Zhang, and M. Sorensen, *J. Am. Chem. Soc.* **2008**, 130, 13202–13203.

8. M. Tang, A. Reichardt, N. Miyaki, R.M. Stoltenberg, and Z. Bao, *J. Am. Chem. Soc.*, **2008**, 130, 6064.

9. D. J. Gundlach, J. E. Royer, S. K. Park, S. Subramanian, O. D. Jurchescu, B. H. Hamadani, A. J. Moad, R. J. Kline, L. C. Teague, O. Kirillov, C. A. Richter, J. G. Kushmerick, L. J. Richter, S. R. Parkin, T. N. Jackson, and J. E. Anthony, *Nat. Mater.* **2008**, 7, 216–221.

10. http://www.rfid-weblog.com/50226711/plastic_rfid_tags_has_their_time_finally_arrived.php

11. http://www.flickr.com/photos/rdecom/4146880795/

12. http://www.hml.queensu.ca/paperphone

13. http://www.ciol.com/Semicon/SemiSpeak/Interviews/E-Inks-electronic-paper-displays-delight!/20808109272/0/

14. Takao Someya, Tsuyoshi Sekitani, Shingo Iba, Yusaku Kato, Hiroshi Kawaguchi, and Takayasu Sakurai, *PNAS*, **2004**, 101, 9966-9970

15. Y. Li, P. Sonar, S. P. Singh, Z. E. Ooi, E. S. H. Lek, and M. Q. Y. Loh, *Phys. Chem. Chem. Phys.*, **2012**, 14, 7162

16. J. N. Haddock, X. H. Zhang, S. Zheng, Q. Zhang, S. R. Marder, and B. Kippelen, *Organic Electronics, 2006*, 7, 45-54

17. J. Chen, and Y. Cao, *Acc. Chem. Res.*, **2009**, 42, 1709–1718

18. J. Roncali, *Chem. Rev*., **1992**, 92, 711–738

19. J. Roncali, *Chem. Rev*., **1997**, 97, 173–205

20. M. Zhang, H. N. Tsao, W. Pisula, C. Yang, A. K. Mishra, and K. Mullen, *J. Am. Chem. Soc.,* **2007**, 129, 3472

21. W. Zhang, J. Smith, S. E. Watkins, R. Gysel, M. D. McGehee, A. Salleo, J. Kirkparick, S. Ashraf, T. Anthopoulos, M. Heeney, and I. McCulloch, *J. Am. Chem. Soc*., **2010**, 132, 11437-11439

22. Y. Hou , G. Long , D. Sui , Y. Cai , and X. Wan, *Chem. Commun*., **2011**, 47, 10401-10403

23. J. D. Yuen, R. Kumar, D. Zakhidov, J. Seifter, B. Lim, A. J. Heeger, and F. Wudl,. *Adv. Mater*., **2011**, 23, 3780-3785

24. Z. Fei, J. S. Kim, J. Smith, E. B. Domingo, T. D. Anthopoulos, N. Stingelin, S. E. Watkins, J. S. Kim, and M. Heeney, *J. Mater. Chem*., **2011**, 21, 16257-16263

25. T. Lei, Y. Cao, Y. Fan, C. J. Liu, S. C. Yuan, and J. Pei, *J. Am. Chem. Soc*. **2011**, 133, 6099

26. J. Mei, D. H. Kim, A. L. Ayzner, M. F. Toney, and Z. Bao, *J. Am. Chem. Soc*., **2011**, 133, 20130–20133

27. Y. Li, S. P. Singh, et al., *Adv. Mater*. **2010**, 22, 4862-4866

28. Z. Chen, M. J. Lee, R. S. Ashraf, Y. Gu, S. A. Seifried, M. M. Nielsen, B. Schroeder, T. D. Anthopoulos, M. Heeney, I. McCulloch, and H. Sirringhaus, *Adv. Mater*. , **2012**, 24, 647–652

29. Y. Li, P. S., S. P. Singh, M. S. Soh, M. Meurs, and J. Tan, *J. Am. Chem. S*oc. **2011**, 133, 2198–2204

30. P. Sonar, S. P. Singh, Y. Li, Z. Ooi, T. Ha, I. Wong, M. S. Soh and A. Dodabalapur*, Energy Environ. Sci.*, **2011**, 4, 2288-2296

31. P. Sonar, S. P. Singh, Y. Li, M. S. Soh and A. Dodabalapur, *Adv. Mater*. **2010**, 22, 5409-5413

32. H. Chen, Y. Guo, G. Yu, Y. Zhao, J. Zhang, D. Gao, H. Liu, and Y. Liu, "Highly π-Extended Copolymers with Diketopyrrolopyrrole Moieties for High-Performance Field-Effect Transistors." *Adv. Mater.* **2012**, DOI: 10.1002/adma.201201318

33. G. Horowitz, *Adv. Mater*., **1998**, 10, 365.

34. C. D. Dimitrakopoulos, and P. R. L. Malenfant, Adv. Mater. 2002, 14, 99.

35. H. E. Katz, *Chem. Mater*., **2004**, 16, 4748.

36. S. Allard, M. Forster, B. Souharce, H. Thiem, and U. Scherf, *Angew. Chem. Int. Ed*. **2008**, 47, 4070.

37. B. S. Ong, Y. Wu, Y. Li, P. Liu, and H. Pan, *Chem. Eur. J*., **2008**, 14, 4766.

38. H. Sirringhaus, M. Bird, T. Richards, and N. Zhao, *Adv. Mater.*, **2010**, 22 3812

39. M. C. Scharber, D. Mühlbacher, M. Koppe, P. Denk, C. Waldauf, A. J. Heeger, and C. J. Brabec, *Adv. Mater.*, **2006**, 18, 789.

40. S. Beaupré, P.-L. T. Boudreault, and M. Leclerc, *Adv. Mater.*, **2010**, 22, E1

41. O. Inganäs, F. Zhang, K. Tvingstedt, L. M.Andersson, S. Hellström, and M. R. Andersson, *Adv. Mater.*, **2010**, 22, E100

42. G. Dennler, M. C. Scharber, and C. J. Brabec, *Adv. Mater.*, **2009**, 21, 1323.

43. B. C. Thompson and J. M. J. Fréchet, *Angew. Chem. Int. Ed*., **2008**, 47, 58.

44. Y.-J. Cheng, S.-H. Yang, and C.-S. Hsu, *Chem. Rev*., **2009**, 109, 5868.

45. J. Yu, M. Abley, C. Yang, and S. Holdcroft, *RSC Chem. Commun*.,**1998**, 1503.

46. J. Yu and S. Holdcroft, *Macromolecules*, **2000**, 33, 5073.

47. Yu, F. P. Orfino, and S. Holdcroft, *Chem. Mater*., **2001**, 13, 526.

48. E. Bundgaard, O. Hagemann, M. Bjerring, N. C. Nielsen, J. W. Andreasen, B. Andreasen, and F. C. Krebs, *Macromolecules*, **2012**, 45, 3644.

49. P. T. Herwig and K. Müllen, *Adv. Mater*., **1999**, 11, 480.

50. A. Afzali, C. D. Dimitrakopoulos, and T. L. Breen, *J. Am. Chem. Soc*., **2002**, 124, 8812.

51. A. R.. Murphy, J. M. J. Fréchet, P. Chang, J. Lee, and V. Subramanian, *J. Am. Chem. Soc*., **2004**, 126, 1596.

52. P. C. Chang, J. Lee, D. Huang, V. Subramanian, A. R. Murphy, and J. M. J. Fréchet, *Chem. Mater*., **2004**, 16, 4783.

53. J. H. Oh, W.-Y. Lee, T. Noe, W.-C. Chen, M. Könemann, and Z. Bao, *J. Am. Chem. Soc.*, **2011**, 133, 4204.

54. J. Liu, E. N. Kadnikova, Y. Liu, M. D. McGehee, and J. M. J. Fréchet, *J. Am. Chem. Soc*., **2004**, 126, 9486.

55. C. Edder, P. B. Armstrong, K. B. Pradob, and J. M. J. Fréchet, *RSC Chem. Commun*., **2006**, 1965

56. M. Bjerring, J. S. Nielsen, N. C. Nielsen, and F. C. Krebs, *Macromolecules*, **2007**, 40, 6012.

57. F. C. Krebs, Solar Energy Mater. *Solar Cells*, **2008**, 92, 715.

58. J. L. Brusso, M. R. Lilliedal, and S. Holdcroft, *Polym. Chem*., **2011**, 2, 175.

59. Y. Li, P. Sonar, S. P. Singh, W. Zeng, and M. S. Soh, *J. Mater. Chem*., **2011**, 21, 10829

60. J. S. Ha, K. H. Kim, and D. H. Choi, *J. Am. Chem. Soc*., **2011**, 133, 10364

61. H. Bronstein, Z. Chen, R. S. Ashraf, W. Zhang, J. Du, J. R. Durrant, P. S. Tuladhar, K. Song, S. E. Watkins, Y. Geerts, M. M. Wienk, R. A. J. Janssen, T. Anthopoulos, H. Sirringhaus, M. Heeney, and I. McCulloch, *J. Am. Chem. Soc*., **2011**, 133, 3272

62. J. D. Yuen, J. Fan, J. Seifter, B. Lim, R. Hufschmid, A. J. Heeger, and F. Wudl, *J. Am. Chem. Soc*., **2011**, 133, 20799

63. J. S. Zambounis, Z. Hao, and A. Iqbal, *Nature*, **1997**, 388, 131.

64. J. Lee , A. Re. Han , J. Hong , J. H. Seo , J. H. Oh, and C. Yang, *Adv. Funct. Mater*., **2012**, DOI: 10.1002/adfm.201200940

65. J. Mizuguchi, A. Grubenmann, G. Wooden and G. Rihs., *Acta Cryst*., **1992**, B48, 696.

66. J. Mizuguchi, *J. Phys. Chem. A*, **2000**, 104, 1817.

67. Y. Li, U.S. Pat. App., 2009 65766 A1, 2009

68. I. McCulloch, M. Heeney, C. Bailey, K. Genevicius, I. Macdonald, M. Shkunov, D. Sparrowe, S. Tierney, R. Wagner, W. M. Zhang, M. L. Chabinyc, R. J. Kline, M. D. McGehee, and M. F. Toney, *Nat. Mater*., **2006**, 5, 328.

69. C. W. Chu, S. H. Li, C. W. Chen, V. Shrotriya, and Y. Yang, *Appl. Phys. Lett*., **2005**, 87, 193508

70. Y. Bai, X. Liu, L. Chen, Khizar-ul-Haq, M. A. Khan, W. Q. Zhu, X. Y. Jiang, and Z. L. Zhang, Microelectronics Journal, 2007,38, 1185-1190

71. Sarma, R. and D. Saikia, *IEEE Electron Device Letters,* **2011**, 32, 209-211

72. A. Buckley, D. Pickup, C. Yates, Y. Zhao, and D. Lidzey, *J. Appl. Phys*., 2011, 109, 084509

73. http://en.wikipedia.org/wiki/Liftoff

74. J. J. M. Halls, C. A. Walsh, N. C. Greenham, E. A. Marseglia, R. H. Friend, S. C. Moratti, and A. B. Holmes, *Nature*, **1995**, 376 498–500

75. G. Yu and A. J. Heeger, *J. Appl. Phys*., **1995** 78 4510–15

76. G. Yu, H. Nishino, A. J. Heeger, T. A. Chen, and R. D. Rieke, *Synth. Met*., **1995**, 72, 249–52

77. E. Moons, *J. Phys-Condens. Matter*, **2002**, 14, 12235-12260

78. R. Shikler, M. Chiesa and R. H. Friend, *Macromolecules*, **2006**, 39, 5393-5399.

79. R. Hamilton, J. Smith, S. Ogier, M. Heeney, J. E. Anthony, I. McCulloch, D. D. C. Bradley, J. Veres and T. D. Anthopoulos, *Adv. Mater.*, **2009**, 21, 1166

80. L. Qiu, J. A. Lim, X. Wang, W. H. Lee, M. Hwang and K. Cho, *Adv. Mater.*, **2008**, 20, 1141.

81. L. Qiu, W. H. Lee, X. Wang, J. S. Kim, J. A. Lim, D. Kwak, S. Lee, and K. Cho, *Adv. Mater.*, **2009**, 21, 1349–1353

Publications

1. <u>Bin Sun</u>, Wei Hong, Hany Aziz and Yuning Li, "Diketopyrrolopyrrole-based semiconducting polymer bearing thermocleavable side chains", *J. Mater. Chem.*, **2012**, 22, 18950-18955

2. Wei Hong, <u>Bin Sun</u>, Hany Aziz, Won-Tae Park, Yong-Young Noh and Yuning Li, "A conjugated polyazine containing diketopyrrolopyrrole for ambipolar organic thin film transistors", *Chem. Commun.*, **2012**, 48, 8413-8415.

3. Yuning Li, <u>Bin Sun</u>, Prashant Sonar and Samarendra P. Singh, "Solution Processable Poly(2,5-dialkyl-2,5-dihydro-3,6-di-2-thienyl- pyrrolo[3,4-c]pyrrole-1,4-dione) For Ambipolar Organic Thin Film Transistors", *Org. Electron.*, **2012**, 13,1606-1613.